



**UNIVERSIDAD AUTÓNOMA  
DE SAN LUIS POTOSÍ  
FACULTAD DE MEDICINA**



**Centro de Investigación en Ciencias de la  
Salud y Biomedicina (CICSaB)**



**FUNCIÓN DE LA GTPasa Npa3 EN LA LEVADURA  
*Saccharomyces cerevisiae***

**TESIS QUE PRESENTA**

MC. MARTÍN ANTONIO MORA GARCÍA

**PARA OBTENER EL GRADO DE DOCTOR  
EN CIENCIAS BIOMÉDICAS BÁSICAS**

CO-DIRECTORES DE TESIS  
DR. ROBERTO SÁNCHEZ OLEA  
DRA. MÓNICA RAQUEL CALERA MEDINA

NOVIEMBRE 2022

## **CRÉDITOS INSTITUCIONALES**

Esta tesis se realizó en el Laboratorio de Biología Molecular y en el Laboratorio de Biología Celular del Instituto de Física de la Universidad Autónoma de San Luis Potosí, bajo la dirección del Dr. Roberto Sánchez Olea y de la Dra. Mónica Raquel Calera Medina. Se agradece el apoyo del Consejo Nacional de Ciencia y Tecnología que otorgó la beca no. 444858 a Martín Antonio Mora García. Para la realización de este trabajo se contó con la aportación del Proyecto de Ciencia Básica Conacyt no. A1-S-21070 (RSO).

Tesis que presenta:

MC. MARTÍN ANTONIO MORA GARCÍA

### **PARA OBTENER EL GRADO DE DOCTOR EN CIENCIAS BIOMÉDICAS BÁSICAS**

CO-DIRECTORES DE TESIS:

Dr. Roberto Sánchez Olea  
Dra. Mónica Raquel Calera Medina

ASESORAS INTERNAS:

Dra. Mariana Salgado Bustamante  
Dra. Esther Layseca Espinosa

ASESORAS EXTERNAS:

Dra. Lina Raquel Riego Ruiz

SINODALES:

Presidente sinodal: Dr. Roberto Carlos Salgado Delgado

Secretaria sinodal: Dra. Esther Layseca Espinosa

Sinodal: Dra. Mariana Salgado Bustamante

Sinodal externa: Dra. Lina Raquel Riego Ruiz

Sinodal suplente: Dra. Othir Gidalti Galicia Cruz

Noviembre 2022



Función de la GTPasa Npa3 en la levadura *Saccharomyces cerevisiae*

por Martín Antonio Mora García

se distribuye bajo una [Licencia Creative Commons Atribución-NoComercial-SinDerivadas 4.0 Internacional](https://creativecommons.org/licenses/by-nc-nd/4.0/).

**Synthetic negative genome screen of the GPN-loop GTPase *NPA3*  
in *Saccharomyces cerevisiae***

Martín Mora-García<sup>1</sup>, Diana Ascencio<sup>2</sup>, Tania Felix-Perez<sup>1</sup>, Judith Ulloa-Calzonzin<sup>2</sup>,  
Alejandro Juarez-Reyes<sup>2</sup>, Karina Robledo-Marquez<sup>3</sup>, Yolanda Reboloso-Gomez<sup>1</sup>,  
Lina Riego-Ruiz<sup>3</sup>, Alexander DeLuna<sup>2\*</sup>, Mónica R<sup>1\*</sup>. Calera, Roberto  
Sanchez-Olea<sup>1\*</sup>.

<sup>1</sup>Instituto de Física, Universidad Autónoma de San Luis Potosí, Av. Manuel Nava no.  
6, Zona Universitaria, 78290 San Luis Potosi, SLP, México.

<sup>2</sup>Unidad de Genómica Avanzada (Langebio), Centro de Investigación y de Estudios  
Avanzados del IPN, Km 9.6 Libramiento Norte Carretera León, 36824 Irapuato,  
GTO, México.

<sup>3</sup>IPICYT, División de Biología Molecular, Camino a la Presa San José 2055, 78216  
San Luis Potosí, SLP, México.

\*Corresponding authors:

Roberto Sánchez-Olea: rsanchez@ifisica.uaslp.mx

Mónica R. Calera: mcalera@ifisica.uaslp.mx

Alexander DeLuna: alexander.deluna@cinvestav.mx

## **Abstract**

The GPN-loop GTPase Npa3 is encoded by an essential gene in the yeast *Saccharomyces cerevisiae*. Npa3 plays a critical role in the assembly and nuclear accumulation of RNA polymerase II (RNAPII), a function that may explain its essentiality. Genetic interactions describe the extent to which a mutation in a particular gene affects a specific phenotype when co-occurring with an alteration in a second gene. Discovering synthetic negative genetic interactions has long been used as a tool to delineate the functional relatedness between pairs of genes participating in common or compensatory biological pathways. Previously, our group showed that nuclear targeting and transcriptional activity of RNAPII were unaffected in cells expressing exclusively a C-terminal truncated mutant version of Npa3 (*npa3 $\Delta$ C*) lacking the last 106-residues naturally absent from the single GPN protein in Archaea, but universally conserved in all Npa3 orthologs of eukaryotes. In order to gain insight into novel cellular functions for Npa3, we performed here a genome-wide Synthetic Genetic Array (SGA) study coupled to bulk fluorescence monitoring to identify negative genetic interactions of *NPA3* by crossing an *npa3 $\Delta$ C* strain with a 4,389-nonessential gene-deletion collection. This genetic screen revealed previously unknown synthetic negative interactions between *NPA3* and 15 genes. Our results revealed that the Npa3 C-terminal tail extension regulates the participation of this essential GTPase in previously unknown biological processes related to mitochondrial homeostasis and ribosome biogenesis.

**Key words:** GTPase Npa3, C-terminal deleted Npa3, Gpn1, synthetic genetic interactions, synthetic lethal, fluorescence, mitochondria, ribosome biogenesis.

## Introduction

GTPases play regulatory functions in many cellular processes, including cell signaling, cell shape, motility and polarity, vesicular or non-vesicular transport and protein synthesis (Leipe et al. 2002; Wittinghofer and Vetter 2011). GTPases are proteins that bind guanosine triphosphate (GTP) and hydrolyze it to guanosine diphosphate (GDP), switching from an inactive state where they are GDP-bound to an active GTP-bound state by exchanging GDP for GTP. The GPN-loop GTPase family, whose name derives from the presence of a strictly conserved GPN (Gly-Pro-Asn) motif, comprises a single GPN protein in Archaea and three orthologs in all eukaryotic organisms: Gpn1 (Npa3 in the budding yeast *Saccharomyces cerevisiae*), Gpn2, and Gpn3. All three proteins are essential for cell viability in yeast, indicating that their functions are not redundant (Giaever et al. 2002; Forget et al. 2010). In yeast and human cells, the best-known biological function of Gpn1, Gpn2 and Gpn3 is to participate in the assembly and subsequent nuclear localization of RNA polymerase II (RNAPII) (Forget et al. 2010; Lacombe et al. 2010; Calera et al. 2011; Minaker et al. 2013; Niesser et al. 2016; Zeng et al. 2018; Liu et al. 2020). Defects in chromatid cohesion, cell cycle progression, and increased sensitivity to DNA-damaging agents are important phenotypes caused by a reduction in GPN proteins function (Forget et al. 2010; Alonso et al. 2011, 2013; Minaker et al. 2013). However, it is challenging to determine if these phenotypes occur downstream of RNAPII transcription inhibition or if they arise from a functional defect in a molecular pathway directly controlled by the GPN proteins that is unrelated to RNAPII function. In a previous study, our group showed that yeast cells expressing exclusively *npa3ΔC*, a

deletion mutant of *NPA3* lacking the C-terminal region that encodes for an approximately 100 amino acid extension present in Gpn1 of all eukaryotes but absent from the single GPN protein in Archaea, proliferated indistinguishably from cells expressing the full-length Npa3 protein. Importantly, the combination of *npa3 $\Delta$ C* mutation with the deletion of *BIK1* (*bik1 $\Delta$* ), a gene that encodes a plus-end tracking microtubule-binding protein with a role in mitotic progression (Berlin et al. 1990), resulted in a synthetic lethal genetic interaction, a result consistent with Npa3 having a role in microtubule dynamics and mitotic progression in an RNAPII-independent manner (Guerrero-Serrano et al. 2017).

A genetic interaction is a phenomenon in which a specific phenotype caused by individual mutations is modified by combining it with another mutation in a second gene (Phillips 2008). A negative extreme form of genetic interaction is synthetic lethality, where two genes that are not essential when mutated or deleted individually are lethal when altered simultaneously (Talavera et al. 2013). Finding negative genetic interactions is useful for identifying functional relationships between genes, as they can reveal information about redundant or compensatory functions, or physical interactions (van Welsem et al. 2008). A powerful tool to discover genetic interactions is the Synthetic Genetic Array (SGA) approach, that allows large-scale screening of genetic interactions in yeast by systematically crossing a query mutant strain with almost all viable deletion mutants to obtain unviable double mutant meiotic progeny (Tong et al. 2001).

Here we used a genome-wide SGA analysis coupled to bulk-fluorescence measurements to search for negative genetic interactions between *npa3ΔC* and a 4,389 nonessential gene-deletion collection in the budding yeast *Saccharomyces cerevisiae*. We identified 15 genes that showed synthetic negative interactions with *npa3ΔC*, which probably include both synthetic lethal and synthetic-sick genetic interactions. Our results suggest that, in addition to its role in RNPAII assembly and nuclear accumulation, *NPA3* participates in cellular pathways related to mitochondrial homeostasis and ribosome biogenesis.



## Materials and methods

### SGA yeast strains and plasmids

*S. cerevisiae* strains used in this study are listed in Table 1. The Mc $\Delta$ 01 (*npa3 $\Delta$ C*) and MCR03 (*NPA3*) SGA starter strains were generated by homologous recombination through a PCR-based approach. To delete the *NPA3* C-terminal tail coding region we used a forward primer (#3) containing 45 bp of homology sequence to the 5' end of the *NPA3* C-terminal tail-coding region followed by a STOP codon. To maintain intact the *NPA3* open reading frame in the MCR03 reference strain, we used a forward primer (#4) containing a 45 bp homology sequence upstream to the *NPA3* native STOP codon. These primers contained a 23 bp-sequence complementary to the 5' end of the NATr cassette. The reverse primer employed to generate both strains contain 45 bp of homology sequence at the 3' end of the *NPA3* ORF (#32), followed by a 23 bp-sequence complementary to the 3' end of the NATr cassette for its amplification from plasmid pYC44 (Yanez-Carrillo et al. 2015). PCR products were transformed by a LiAc/ssDNA/PEG protocol (Castano et al. 2003) in the *S. cerevisiae* parental strain YEG01-RFP constitutively expressing the red fluorescence protein (RFP) mCherry linked to *hphMX4* selection marker at the *PDC1* locus. Correct replacement of *NPA3* C-terminal tail coding region by the NATr cassette in Mc $\Delta$ 01 strain, and NATr cassette insertion immediately after the STOP codon (TAA) of the *NPA3* ORF in MCR03 strain, was verified by amplifying PCR products of the expected size with primers complementary to upstream (#8/#9) and downstream (#10/#11) regions of the deletion/insertion region within the genome. We used flanking primers (#8/#10) for PCR amplification of the NATr cassette from

genomic DNA from Mc $\Delta$ 01 and MCR03 strains. To unambiguously confirm that the deletion/insertion occurred through homologous recombination at the *NPA3* locus, PCR products from both strains were sequenced with #123/#124 primers at LANBAMA, IPICYT (primers used are listed in Table 2). We used 4,389 nonessential-gene knockouts from the yeast deletion collection (BY4741 genetic background) (Winzeler et al. 1999) for our systematic screening of genetic interactions.

### **Synthetic Genetic Array (SGA) coupled to bulk-fluorescence data collection**

We developed a bulk-fluorescence based approach to assess yeast colony growth. To this end we took advantage of the red fluorescent protein mCherry (RFP), which is expressed constitutively by the YEG01-RFP strain and used the fluorescence values as a proxy for colony growth. We coupled this bulk-fluorescence approach to previously reported SGA methodology (Tong and Boone 2006). Replica pinning steps were performed manually with a 384-head pin tool (V&P Scientific, VP384F). For the single-mutant selection step, the cells were plated and incubated at 30 °C for 24 h, measured for RFP signal and replica plated to double-mutant selection media (Supplementary Table 1). For the double mutant selection step the cells were incubated at 30 °C for 48 h and the RFP signal was measured as described. Data from SGA colonies were collected by reading the red fluorescence signal in each array position with 15 flashes at 400 Hz and 100 gain value in the RFP channel, using a micro plate reader Infinite M1000, TECAN (Ex 587 nm/5 nm and Em 610 nm/5 nm). Background fluorescence signal was collected from single-well plates

(OmniTray, Nunc) containing selective media but with no cells. Raw fluorescent signal for each SGA position was defined as:  $F_{x_{raw}} - F_{bg} = F_x$ . To identify negative genetic interactions with the *npa3ΔC* mutation we first made 5 repetitions of a genome-wide screening by crossing the McΔ01 strain with a collection of 4,389 non-essential gene deletion strains. On the basis of the first screening results, we then performed 11 repetitions of a high-resolution analysis in which we crossed the McΔ01 strain with the arrayed genes scored as putative synthetic negative interactions from the genome-wide screening, and crossing in parallel, but independently, the MCR03 reference strain with the same array.

### Data analysis

To evaluate synthetic negative interactions among nonessential genes and *npa3ΔC* we related the colony RFP signal value from double mutants to single mutant values, assuming that if there are not genetic interactions the multiplicative combination of single-mutant fitness and experimental factors will represent the double-mutant fitness. We employed normalization procedures to estimate and remove systematic biases in colony growth that arise from experimental factors. In the genome-wide screening the normalization was first made by subtracting the median  $F_x$  value from not-empty positions per plate to  $F_x$  values in each plate:  $F_x - (\text{median}(F_x(\text{plate}))) = F_{p_x}$ , followed by subtraction of the median value of the same well to the same well position in all plates:  $F_{p_x}(\text{well}) - (\text{median}(F_{p_x}(\text{well}))) = FN_x$ .

On the base of the normalized fluorescence values, we generated a viability matrix that precisely indicated which position in the 5 replicas of the SGA array presented either proliferation or no colony growth. Then, we were able to set a condition for identifying putative synthetic negative interactions. The haploid strains able to proliferate (present) in at least 3 of 5 SGA replicates on selective media containing G418, but showing no growth (completely absent) in at least 2 of these identical 3 SGA replicates on selective media containing both G418 and clonNAT antibiotics, were scored as displaying a putative synthetic negative growth phenotype. Approximately, 564,000 data generated from red fluorescence reading and normalization steps were processed with MATLAB (software version 7.10).

Normalization procedure for the two SGA experiments (Mc $\Delta$ 01 and MCR03) within the high-resolution analysis was done by subtracting the background values, followed by normalizing with the median value per plate of all *ho* $\Delta$  positions:  $F_x(\text{well}) - (\text{median}(F_{ho\Delta}(\text{plate}))) = FN_x$ . Then, the negative effect in growth was represented by negative deviations from the expected double-mutant fitness. To assess negative genetic interactions for each SGA experiments, we calculated an interaction score by subtracting the respective fluorescence values of MCR03 experiment from the respective fluorescence values of the Mc $\Delta$ 01 experiment:  $FN_x(\text{Mc}\Delta 01) - FN_x(\text{MCR03}) = \text{genetic interaction score (GIS)}$ . Finally, to determine if the differences between the Mc $\Delta$ 01 experiment and reference MCR03 experiment were statistically significant we applied a student t-test (GIS vs MCR03). Data from high-resolution analysis were processed with RStudio (software version 1.2.5033).

## Study of synthetic negative interactions *de novo* by plasmid shuffling

To further characterize the selective synthetic negative interactions of *npa3ΔC* with *bud27Δ* identified in our study, we employed a plasmid shuffling strategy in the *S. cerevisiae* BY4741 strain, an intact isogenic parental background to the YEG01-RFP strain used in our SGA analysis. First, cells were transformed with a pRS416-*NPA3* (*URA3*) maintenance plasmid. Then, through a PCR-mediated gene targeting approach, the endogenous *NPA3* gene was replaced by the *natMX4* cassette obtained from the plasmid pYC44 with forward (#84) and reverse (#4) primers. After the deletion of *NPA3* was confirmed by sequencing using #123 and #124 primers, we used the *kanMX4* cassette obtained by PCR from the pFA6 plasmid with forward (#89) and reverse (#90) primers to delete *BUD27*. Once *BUD27* deletion was confirmed by sequencing using the #105 and #106 primers, we transformed this strain with the second plasmid pRS315 (*LEU2*) carrying *NPA3* (BYMG56 strain) or *npa3ΔC* (BYMG57 strain). Both strains were grown at 30 °C and 200 rpm in liquid SCM -Leu medium (0.67% YNB w/o amino acids, 2% dextrose, and 0.2% amino acid drop-out -leu) for 24 h. Then, cells were diluted by 1000-fold in the same SCM-Leu medium and grown in the same conditions for another 24 h. We repeated this dilution and growth in fresh media one more time. Finally,  $\sim 10^4$  cells from the last culture were spread onto the indicated plates containing the appropriate selection media to test for the possible loss of pRS416-*NPA3* (*URA3*) maintenance plasmid. This included plates with SCM -Leu medium and 5-FOA counter selection SCM/5-FOA medium (0.67% YNB w/o amino acids, 2% dextrose, 0.2% amino acid drop-out -ura, 50 μg/mL uracil and 0.1% 5-fluoroorotic acid).

## **Identification of co-expression profiles of *NPA3* synthetic negative interactors and GO enrichment analysis**

To identify genes co-expressed with *npa3ΔC* synthetic negative interactors across all transcriptomics datasets deposited in the yeast *Saccharomyces* genome database (SGD), the Serial Pattern of Expression Levels Locator database (SPELL) (Hibbs et al. 2007) was queried with the 15 synthetic negative interacting genes reported here and *NPA3* gene with the online interface provided at SGD (<https://spell.yeastgenome.org>). We arbitrarily consider for the subsequent analysis the set of genes co-expressed with *npa3ΔC* synthetic negative interactors and *NPA3* gene that displayed an adjusted correlation score  $\geq 1.4$ . Then, functional enrichment analysis was performed with the g:Profiler web server (<https://biit.cs.ut.ee/gprofiler/gost>) (Raudvere et al. 2019), using biological process annotations from gene ontology (GO). The co-expressed genes obtained from SPELL, together with the 15 *npa3ΔC* synthetic negative interactors and *NPA3* were set as an unranked target list, and the complete *S. cerevisiae* genome from Ensembl Genomes (<http://ensemblgenomes.org/>) was set as the background list. Network representation was created using Cytoscape 3.8.2 (Shannon et al. 2003).

## **Identification of genes with genetic interaction profiles similar to *NPA3***

We searched TheCellMap web server (<https://thecellmap.org/>) to identify genes displaying a similar genetic interaction profile to *NPA3*. We fed the search toolbar with the *NPA3* gene name and set the Pearson's coefficient cutoff in 0.2, as recommended by the authors of this tool (Usaj et al. 2017).

## Cell growth assays

In order to evaluate the effects of stressors on cell growth, we generated the strains BYMG20 (*NPA3*), BYMG21 (*npa3ΔC*) and BYMG34 (*npa3ΔC/NPA3*). These strains were grown in selection media (0.17% YNB w/o amino acids and ammonium sulfate, 0.1% MSG, 2% dextrose, 100μg/mL clonNAT and 2% amino acid drop-out -Leu or -Leu/Ura, respectively) to stationary phase, adjusted to an  $OD_{600} = 0.4$  and serially diluted by 10-fold. To examine the strains' response to a ribosome biogenesis stressor or to a mitochondrial damage-inducing agent, we spotted the cells array, using the multi-blot replicator VP 407AH (V&P Scientific), onto YPD plates containing 15 μM actinomycin D (Sigma-Aldrich) or 24 μg/mL ethidium bromide (Bio-Rad).

## Evaluating the expression levels of the retrograde response genes *CIT2*, *IDH1* and *IDH2* by real time PCR

BY4741 (parental), BYMG20 (*NPA3*) and BYMG21 (*npa3ΔC*) yeast strains were grown overnight in liquid SCM (0.17% YNB w/o amino acids and ammonium sulfate, 0.1% MSG, 2% dextrose and 2% all amino acid mix) and SCM -Leu +NAT media (0.17% YNB w/o amino acids and ammonium sulfate, 0.1% MSG, 2% dextrose, 100μg/mL clonNAT and 2% amino acid drop-out -Leu), respectively, with shaking (180 rpm) at 30 °C. Cells were spun down, washed and resuspended in 500 μL of sterile milliQ water. Then, all three strains were inoculated in 50 mL of their corresponding fresh liquid media to an adjusted  $OD_{600} = 0.005$  and incubated at 30 °C with shaking (180 rpm) until cultures reached an  $OD_{600} = 0.8$ . Cells were spun down, washed and resuspended in 500 μL of sterile milliQ water. Thereafter, each

strain was inoculated in 60 mL of liquid YPD (1% Bacto-yeast extract, 2% bacto-peptone and 2% dextrose) to an adjusted  $OD_{600} = 0.4$ ; cultures were incubated at 30 °C with shaking (180 rpm) during 4 h. Cells were then pelleted and total RNA was extracted as described previously by Schmitt et. al. (Schmitt et al. 1990). RNA was treated with Turbo DNase (Ambion) and cDNA synthesis was made with the Superscript II reverse transcriptase kit (Invitrogen) with oligo (dT)18. qPCR was performed using SYBR Green Master Mix (Radiant) in a Piko Real 96 Real Time PCR System (Thermo-Scientific). Primers (indicated in Table 2) used for the real time PCR were forward #125 and reverse #126 for *CIT2*, forward #127 and reverse #128 for *IDH1*, forward #129 and reverse #130 for *IDH2*, and forward #131 and reverse #132 for *ACT1*. Gene expression of *ACT1* was used as a normalization control. The experiment was performed in triplicate and two-way ANOVA followed by Tukey's multiple comparisons test was performed using GraphPad Prism (version 8.4.0, GraphPad Software, San Diego, California USA).



## Results

### **Development of a bulk-fluorescence based high-throughput approach to identify negative genetic interactions with *npa3ΔC***

Methods based on pixel analysis that approximate yeast growth have demonstrated to be very useful to identify genetic interactions in high-throughput analyses (Tong et al. 2001; Jorgensen et al. 2002). However, high resolution of screens based on colony size require massive number of replicates for scoring synthetic effects (Roguev et al. 2007). We have successfully used bulk measurements of constitutively expressed fluorescence reporters as a proxy for fitness, allowing for higher resolution (DeLuna et al. 2008; Garay et al. 2014). Fluorescence proteins constitute a widely used tool that enables the visualization and evaluation of numerous cellular processes in yeast (Higuchi-Sanabria et al. 2016). Yeast cells are capable to produce fluorescent proteins regardless of their position within the colony (Steff et al. 2001), and this signal can be efficiently collected from the center and edges of that colony. Finally, detection of the fluorescence signal by high performance instruments allows the assessment of colony growth in a larger dynamic range than using pixels, providing a quick means to unambiguously score strong growth defects. Here, we used a bulk-fluorescence based high-throughput approach to assess yeast colony growth employing a yeast strain constitutively expressing the mCherry protein fused to the strongly, constitutively expressed Pdc1 protein.

Here, we applied this SGA coupled to bulk-fluorescence method to perform a genome-wide search to identify genes showing synthetic negative interactions with the *npa3ΔC* deletion mutant. First, we generated an SGA query strain harboring the *npa3ΔC* mutation in the chromosome (McΔ01). A PCR-based homologous recombination strategy was employed to replace the *NPA3* C-terminal tail region with the NATr cassette. Although the *natMX4* marker is neutral for fitness (Sliwa and Korona 2005), we also generated as a negative control a reference strain (MCR03) in which we introduced the NATr cassette at the *NPA3* locus after the stop codon, leaving intact the *NPA3* coding region (Figure 1A). The integration site of the selection marker in the genome was first verified through a PCR strategy in both strains (McΔ01 and MCR03). We designed primers pairing ~100 bp upstream and downstream of the expected recombination site for both 5' and 3' junctions of the NATr cassette in the genome (Supplemental Figure 1). The amplification of a DNA fragment of the expected size confirmed that the integration site of the NATr cassette had occurred by homologous recombination at the *NPA3* locus (data not shown). Second, in both strains we performed direct sequencing of a PCR product containing the integration site. In addition, McΔ01 and MCR03 strains were tested for the appropriate auxotrophic and antibiotic-resistance markers. The proliferation rate of both McΔ01 and MCR03 strains was similar to the parental strain, indicating that the insertion of the NATr cassette in the genome had no effect on this parameter (Figure 1B).

### **Genome-wide screening for putative *npa3ΔC* synthetic negative interactions**

We then proceed to systematically cross the McΔ01 query strain (*MATα*, clonNAT resistant) with an array of *MATa* deletion mutants in 1 of 4,389 nonessential *S. cerevisiae* genes harboring a G418 selection marker. As a result, we obtained G418/clonNAT resistant diploids that were sporulated and selected on haploid-specific media. To increase the resolution of the double-knockout profiling, we took advantage of the mCherry (RFP) bulk-fluorescent marker present in the parental query strains. Based on the distribution of the normalized fluorescence values, from the KanR and KanR NatR selection steps, we obtained a viability matrix by setting the  $-1.5 FN_x$  value as detection threshold for growth colony ( $>-1.5$ =present,  $<-1.5$ =absent) (Figure 2). Synthetic negative interactions were identified by detecting double mutants with an aggravated phenotype (KanR NatR selection) compared with each of the corresponding array single mutants' phenotype (KanR selection). Based on this definition, we expected that in the absence of negative genetic interactions, there would not be any difference between single and double mutant growth. Thus, positions showing highly diminished normalized fluorescence values in the double mutant selection step compared to the single mutant selection step were considered as putative synthetic negative interactions (Figure 3). To identify with high confidence synthetic negative interactions, we look for positions in which at least 3 of 5 colonies were present in the KanR single mutant selection step, and that, for the same position, at least 2 of the 5 colonies were absent in the KanR NatR selection step for the double-mutant. Based on this criterion, we identified 83 nonessential genes displaying a putative negative synthetic interaction with the Npa3 C-terminal tail coding region deletion mutant

(Table 3; viability matrix is presented in Supplemental Data 1). Remarkably, among the putative synthetic lethal genes with *npa3ΔC* we detected the 4 closest neighbors to the *NPA3* locus in the genome: *MOG1*, *OPI3*, *LIA1* and *HAM1*. Although these genes do not really represent true genetic interactions with *npa3ΔC*, it is an expected result due to the improbability of segregating these genes from *NPA3* during the crosses. The identification of these genes in our genome screen gives support and credibility to the appropriateness of our experimental system to identify genes interacting negatively with *npa3ΔC*.

### **Confirming *npa3ΔC* synthetic negative interactions at a higher statistical resolution**

To confirm the *npa3ΔC* negative synthetic interactions obtained in our screen we performed a high-resolution analysis in which we arrayed the 83 putative hits obtained in the genome-wide screening described above and crossed them again to the McΔ01 query strain. This time, we also included a strain harboring a neutral mutation (*hoΔ::kanMX4*) homogeneously distributed in 75% of the 384 positions' array. RFP-mCherry signal collected from this control showed the single mutant growth phenotype of the query strain (Baganz et al. 1997). Considering that the formation of haploid double mutants by meiotic recombination is highly unlikely if the two genes to be combined are tightly linked in the same chromosome (Kaboli et al. 2014), we included as positive controls in the target array the 4 deletion mutant strains in the closest loci to *NPA3* (*mog1Δ::kanMX4*, *opi3Δ::kanMX4*, *lia1Δ::kanMX4* and *ham1Δ::kanMX4*), as a reference for no colony growth phenotype. As expected,

these 4 mutants displayed a synthetic lethal-like phenotype when combined with the *npa3ΔC* mutation in the genome-wide SGA. In addition, we included the *iwr1Δ::kanMX4* mutant due to the previously reported physical interactions of Iwr1 with several subunits of the RNAPII complex (Krogan et al. 2006), and the genetic interactions described for *IWR1* with *BUD27* and *GPN2*, two genes involved in RNAPII biogenesis and nuclear import (Scherrer et al. 2011; Minaker et al. 2013). To discard a possible slow growth phenotype caused by the presence of the NATr cassette at the *NPA3* locus, we also crossed the same target array with the MCR03 query strain and considered it as a reference SGA. The same experimental methodology for the SGA coupled to bulk-fluorescence we described above, was followed for both experiments, McΔ01 and MCR03 (Figure 4). Then, we normalized the fluorescence values obtained from the single-mutant and double-mutant selection steps (Supplemental Figure 2). Thereafter, we used those normalized fluorescence values to generate a genetic interaction score to qualitatively represent cell growth and identifying those double mutants showing a negative effect in growth, as compared to single mutants.

As we designed the SGA coupled to bulk-fluorescence for high-resolution detection of negative genetic interactions in budding yeast, we discarded double-mutants that displayed a positive interaction-like phenotype, showing GIS values >0 (over the reference *hoΔ/npa3ΔC* GIS value). However, negative GIS values provide a qualitative representation of the detrimental biologic effect in growth phenotype caused by the combination of a nonessential-gene deletion and the *npa3ΔC* mutation. Next, we arbitrarily set a stringent cut-off to score synthetic negative

interactions with *npa3ΔC* (Figure 5). Below this GIS cut-off value we identified *BUD27*, *GIS2*, *ARC18*, *PPT2*, *RAD6* and *MTC7*, as genes interacting negatively with *npa3ΔC*. Noteworthy, 3 (*MOG1*, *LIA1*, and *HAM1*) of the 4 genes included in the array as positive controls for the experiment displayed GIS values below the stringent cut-off. Additionally, we also set a lenient cut-off GIS value to include *OPI3*, the fourth gene considered as positive control in our study. This more relaxed GIS cut-off allowed the inclusion of double-mutants with a less pronounced but still clear detrimental effect on cell growth. Among the genes belonging to this group were *DLD3*, *IWR1*, *PUF4*, *SIC1*, *MSW1*, *CCC2*, *RMD9*, *MRPL37* and *SPG3*. To test if the differences obtained were statistically significant, we employed a student t-test (Supplemental Data 2). Altogether, through our SGA coupled to bulk-fluorescence analyses, we identified 15 synthetic mutations with *npa3ΔC* that displayed a synergistic negative effect in cell growth, which probably include both synthetic lethal and synthetic-sick genetic interactions (Figure 5). We identified genes that showed synthetic negative interactions with *npa3ΔC* that regulate different aspects of transcription, including *IWR1*, *BUD27*, *PUF4* and *GIS2*. In addition, we identified negative interactions between *npa3ΔC* and genes regulating the cell cycle (*SIC1*) and protein degradation and DNA repair (*RAD6*). Interestingly, we identified a synthetic negative interaction of *npa3ΔC* with *SPG3*, a gene of unknown function but apparently related to carbon assimilation, and *MTC7*, a gene likely to be involved in ribosome biogenesis, as its function has been linked to *BUD21*, a gene involved in rRNA processing (Schlitt et al. 2003).

Unexpectedly, several of the synthetic negative interactions we report here for *npa3ΔC* are with genes encoding mitochondrial proteins that play important roles in mitochondrial vital biosynthetic processes (*PPT2*), localization of mitochondria in the cell (*ARC18*), mitochondrial translation machinery (*MRPL37* and *MSW1*), and the control of mitochondrial gene expression (*RMD9*) (Myers and Tzagoloff 1985; Grohmann et al. 1991; Fehrenbacher et al. 2005; Stenger et al. 2020). *npa3ΔC* also displayed a negative synthetic interaction with *DLD3*, a gene encoding a cytoplasmic protein that is a member of the retrograde regulon, a set of nuclear genes whose transcription is upregulated by damaged mitochondria (Chelstowska et al. 1999), and with the trans-Golgi cooper transporter *Ccc2* and *Gis2*, two additional proteins with a mitochondrial function. Interestingly, *ccc2Δ* mutant cells also exhibited defects in respiration (Yuan et al. 1995) and *GIS2* is a modulator of ribosomal translation of mitochondrial precursor protein synthesis (Seidel and Meierhofer 2017), thus having a role in the two larger groups of *NPA3* interacting genes, one involved in ribosome biogenesis and the other in mitochondrial homeostasis.

### **Study of the synthetic negative interaction of *npa3ΔC* with *bud27Δ* *de novo* by plasmid shuffling**

Secondary assays are always recommended to verify novel negative genetic interactions due to intrinsic features of the SGA method that may cause a synthetic silencing effect (Hughes et al. 2000; van Welsem et al. 2008). We decided to further verify the synthetic negative interaction of *bud27Δ* with *npa3ΔC* by generating double mutants *de novo* using homologous recombination followed by the plasmid shuffling

technique (Boeke et al. 1987). To this end, we generated the double chromosomal mutant *npa3Δ/bud27Δ* carrying an *NPA3-URA3* maintenance plasmid together with a second *NPA3-LEU2* or *npa3ΔC-LEU2* plasmid. Strains were grown as described in Materials and methods in selective media containing uracil but lacking leucine (SCM -Leu). This media selects for the presence of the *LEU2* carrying plasmids and simultaneously releases any negative selection in the growth of cells that spontaneously lose the *NPA3-URA3* rescue plasmid (Ura<sup>-</sup> cells). The resulting cells were plated onto SCM -Leu and SCM/5-FOA plates to evaluate the rate of loss of the *NPA3-URA3* rescue plasmid. If the *npa3ΔC* mutant carried in the *LEU2* plasmid will render only inviable Ura<sup>-</sup> *npa3Δ/bud27Δ* cells, then no colony growth will be seen at 5-FOA containing plates (Figure 6A). Confirming the SGA result, cells harboring *npa3ΔC-LEU2* plasmid in combination with the double chromosomal mutant *npa3Δ/bud27Δ* were not able to form regular colonies. In contrast, *npa3Δ/bud27Δ* cells harboring the *NPA3-LEU2* plasmid formed numerous colonies (Figure 6B). This result confirms the synthetic negative interaction between *npa3ΔC* and *bud27Δ* we observed in the SGA analysis and showed that this interaction corresponds to the extreme form of synthetic lethality.

### ***NPA3* synthetic negative interactors co-expression profiles network**

Genetic interactions regulating a phenotype within cells can be mediated by several mechanisms and involve different types of biomolecules including mRNA, proteins, or metabolites (Costanzo et al. 2010, 2016). Thus, we reasoned that exploring co-expression profiles might contribute to gain more insight into a possible common



function for *NPA3* and the synthetic negative genes with *npa3ΔC* in specific biological processes. To this end, we queried the SPELL section in SGD to identify the set of genes whose expression is co-regulated with the set of genes of our interest. We obtained 123 genes showing similar co-expression profiles with *NPA3* and the *npa3ΔC* synthetic negative interactors from this SPELL analysis (Supplemental Data 3). Thereafter, to identify the biological processes that were significantly enriched in the set of genes containing the 15 synthetic negative interactors with *npa3ΔC*, the top 123 co-regulated genes and *NPA3*, we performed a functional enrichment analysis. This analysis showed an enrichment of biological processes related to ribosome biogenesis and function, revealing a previously unknown functional relationship of *NPA3* with those biological processes (Figure 7).

### ***NPA3* profile similarity subnetwork**

A gene function can be inferred by assessing its genetic interaction profiles. These profiles include both the set of negative and positive genetic interactions for a particular gene. A high similarity in the genetic interaction profiles of two given genes may indicate that these genes participate in the same biological processes, pathway(s), and/or protein complex (Costanzo et al. 2010, 2016). To extend our observations on *NPA3* by assessing orthogonal functional data, we searched the TheCellMap genetic interactions server to identify those genes in yeast with a genetic interaction profile most similar to *NPA3*. The quest in the TheCellMap repository revealed only 3 genes with a significant genetic interaction profile similar to *NPA3*, namely *UTP23*, *SAM35* and *CDC10* (Figure 8). *UTP23* encodes an

essential protein component of the small subunit processome involved in 40S ribosomal subunit biogenesis (Hoareau-Aveilla et al. 2012), which incidentally has also been described in high-throughput studies to localize to mitochondria. Sam35 is a pivotal component of the sorting and assembly machinery complex (SAM) located in the mitochondrial outer membrane (Milenkovic et al. 2004; Paschen et al. 2005). Finally, Cdc10 is a subunit of the septin complex with GTPase activity involved in cytokinesis, polarity and morphogenesis (Field and Kellogg 1999; Costanzo et al. 2010, 2016), but that in addition is required for efficient trafficking of CoQ to mitochondria (Fernández-Del-Río et al. 2020). A similarity in the genetic interactions of *NPA3* with *UTP23*, *SAM35* and *CDC10* supports our proposal, based on the *npa3ΔC* negative interacting genes obtained in our SGA and the biological processes enriched with these genes, as well as the SPELL co-expression data, that Npa3 cellular function is integrated with mitochondrial function and ribosome biogenesis.

### ***npa3ΔC* cells growth is more sensitive to actinomycin D and ethidium bromide than cells expressing full-length Npa3**

As mentioned above, most genes identified in SPELL as being co-regulated with *NPA3* and some of the *npa3ΔC* synthetic negative-interacting genes play a recognized role in ribosome biogenesis. This observation points to the interesting possibility that Npa3 might also be involved in ribosome biogenesis. To start generating experimental evidence in support of this hypothesis, and considering that strains from the yeast deletion collection may carry nonlinked mutations that may affect phenotypic characterization (Hughes et al. 2000), we generated the strains

BYMG20 (*NPA3*), BYMG21 (*npa3ΔC*) and BYMG34 (*npa3ΔC/NPA3*) to evaluate the effects of some stressors on cell growth. Then, we compared the sensitivity of *npa3ΔC* and *NPA3* cells growth to actinomycin D (ActD), an inhibitor of RNA polymerase I (Perry and Kelley 1970), and therefore, of ribosomal RNA synthesis. If the *npa3ΔC* mutant allele is unable to support an optimal level of ribosome biosynthesis, regardless of the specific step, we expect to observe an increase in the sensitivity of *npa3ΔC* cells growth to ActD, in comparison with *NPA3* cells. Indeed, as shown in figure 9A, growth of *npa3ΔC* cells was clearly more sensitive to ActD than that of *NPA3* cells. Importantly, this increase in sensitivity was suppressed by an episomal expression of full-length Npa3, confirming that this effect was specifically due to a functional deficiency in the *npa3ΔC* mutant allele.

On the other hand, results of our SGA study also showed that *npa3ΔC* interacts with genes encoding mitochondrial proteins that play important roles in mitochondrial translation, metabolism, localization, and gene expression. It is known that contributions from both, nuclear and mitochondrial genomes, are indispensable for the maintenance of mitochondrial function during cell growth and development (Grivell 1995; Maity and Chakrabarti 2021). Several studies have used the intercalating agent ethidium bromide as a selective inhibitor of mitochondrial DNA (mtDNA) synthesis to explore mitochondrial cellular functions (Goldring et al. 1970; Hobbs et al. 2001; Chen et al. 2005; Luévano-Martínez et al. 2015). To gain insight into a possible Npa3 mitochondrial related function, we evaluated the effect of ethidium bromide on the proliferation of *npa3ΔC* and *NPA3* cells (Figure 9B). As expected, *npa3ΔC* cells growth displayed an increased sensitivity to the inhibitory effect of

ethidium bromide. Importantly, this effect was reversed by episomally expressing Npa3 wt. These results support the proposal that Npa3 may play a role in the cellular response to mitochondrial dysfunction.

### **Expression of the retrograde pathway marker *IDH2* is increased in *npa3ΔC* cells**

In our SGA study we obtained several genes interacting with *npa3ΔC* that encode mitochondrial proteins. These results raised the possibility that *npa3ΔC* cells may have a subtle mitochondrial deficit that adds to a minor negative effect caused by the absence of one of these gene products to cause the *xxxΔ/npa3ΔC* synthetic negative interaction. Our result showing that *npa3ΔC* cells growth displayed a higher sensitivity to the inhibitory effect of ethidium bromide is consistent with that proposal. Mitochondrial dysfunction activates a retrograde pathway that leads to an increased expression of a set of nuclear genes (Butow and Avadhani 2004; Liu and Butow 2006). Thus, we employed real time PCR to investigate if the expression of the classical retrograde markers *CIT2*, *IDH1* and *IDH2* was increased in *npa3ΔC* cells. As shown in figure 10, *CIT2* expression was unaffected in *npa3ΔC* cells but the expression of *IDH2* was significantly increased in *npa3ΔC* cells compared to both, *NPA3* control cells and unmodified BY4741 parental cells. The expression of *IDH1* was significantly increased in *npa3ΔC* cells compared to BY4741 cells, but although *IDH1* expression was higher in *npa3ΔC* than *NPA3* cells, the difference was not statistically significant. Thus, a marked increase in *IDH2* but not *CIT2* expression in

*npa3ΔC* cells points to an alteration in mitochondrial physiology that leads to the activation of a cell response that is different from the classical retrograde pathway.

## Discussion

Here we took advantage of the absence of a strong growth phenotype in the  $Mc\Delta 01$  strain to search for synthetic negative genetic interactions of a C-terminal deleted Npa3 mutant,  $npa3\Delta C$ , by combining the  $npa3\Delta C$  mutation within an RFP-expressing strain with one deletion mutant from the nonessential gene-deletion yeast collection. In this study, we were able to identify and confirm synthetic negative interactions with  $npa3\Delta C$  in a high-throughput manner by coupling detection of bulk-red fluorescence to SGA methodology. Independently that this variation of the SGA method we implemented here may be improved, we suggest, based on the evidence presented in this work, that SGA analysis coupled to bulk-fluorescence is a reliable method to search for negative genetic interactions in budding yeast. Our plasmid shuffling experiments verified the  $npa3\Delta C/bud27\Delta$  negative genetic interaction *de novo*, and revealed that this belongs to the most extreme form of interaction called synthetic lethality. This result, together with the appearance in our study of the *NPA3* neighboring genes as apparent negative interacting genes, gives strong credibility to our study. However, more experimental work is needed to verify the other genetic interactions obtained for  $npa3\Delta C$  in our SGA analysis, as we selected the  $npa3\Delta C/bud27\Delta$  combination to confirm *de novo* because it was the interaction that displayed the highest GIS value.

Npa3, Bud27 and Iwr1 are involved in RNAPII assembly and nuclear targeting (Forget et al. 2010; Czeko et al. 2011; Miron-Garcia et al. 2013; Zeng et al. 2018), suggesting that the  $npa3\Delta C$  negative genetic interactions may result from an

impairment in RNAPII biogenesis. Additionally, the results of SPELL showing a co-regulation of *NPA3* expression with genes involved in ribosome biogenesis or function might point to a defect in these processes as a probable explanation for the synthetic negative interactions we identified here for *npa3ΔC*. However, we propose that the *npa3ΔC* genetic interactions we identified here are not likely due to Npa3's role in RNAPII assembly, as we have previously shown that RNAPII nuclear targeting and activity were unaffected in *npa3ΔC* cells (Guerrero-Serrano et al. 2017), but more reveal additional, still to define, novel functions of Npa3 in diverse cellular processes. A putative deficiency of RNAPII in *npa3ΔC*, if any, is not enough to affect cell proliferation in *npa3ΔC* cells (this work). Indeed, Bud27 also regulates the assembly of RNA polymerase III (RNAPIII), and both Npa3 and Bud27 were identified by mass spectrometry as proteins associated to this enzyme (Vernekar and Bhargava 2015; Bhalla et al. 2019), raising the possibility that they may cooperate to regulate RNAPIII. A functional regulation of any aspect of RNAPIII by Npa3 may potentially explain the co-regulation of *NPA3* expression with a set of genes involved in ribosome biogenesis, as RNAPIII synthesizes rRNA 5S. Additionally, Bud27 is also involved in translation initiation (Deplazes et al. 2009), raising the possibility that synthetic lethality in *npa3ΔC/bud27Δ* might be due to a potential involvement of Npa3 in translation, an interesting possibility worth testing experimentally.

Among the negatively interacting genes with *npa3ΔC* not only *BUD27* participates in ribosome biogenesis (Martínez-Fernández et al. 2020), but also other genes found in our study play important roles in this biological process. *PUF4*, codes for a protein that preferentially binds to mRNAs encoding nucleolar rRNA-processing factors and

mRNAs encoding proteins that participate in ribosome biogenesis (Wickens et al. 2002; Gerber et al. 2004; Lapointe et al. 2017). *GIS2* associates with functionally related groups of mRNAs coding for proteins involved in ribosome biogenesis (Scherrer et al. 2011). Finally, *MTC7* is also likely to play a role in ribosome biogenesis (Schlitt et al. 2003). Interestingly, Npa3 was identified by mass spectrometry as an Npa1-associated protein and given the name of “Nucleolar Preribosomal Associated protein 3” or Npa3, as Npa1 associates with the pre-60S ribosomal particle. Any role of Npa3 in ribosome biogenesis was quickly discarded mainly based on the cytosolic localization observed for this protein (Dez et al. 2004). In addition, the results of our search in SPELL revealed that there is a clear co-regulation of *NPA3* expression with genes involved in ribosome biogenesis, further supporting a possible role for Npa3 in this process. Moreover, our results showing a higher sensitivity of *npa3ΔC* than *NPA3* cells to the RNA polymerase I inhibitor actinomycin D (ActD) is also consistent with a role in ribosome biogenesis. Although we cannot rule out that the higher sensitivity of *npa3ΔC* cells to ActD is due to inhibition of RNA polymerase II (RNAPII), we believe this is unlikely as a higher concentration of ActD (20μM) than the one we employed here (15 μM) had no effect on the induction of a protein reporter gene in *S. cerevisiae* (Gorenstein et al. 1978), a process requiring mRNA synthesis by RNAPII. More importantly, as we mentioned above, the Npa3 C-terminal tail is not required for proper nuclear targeting or activity of RNAPII, as both were undistinguishable between *npa3ΔC* and *NPA3* cells (Guerrero-Serrano et al. 2017). Altogether, the novel genetic interactions we uncovered here for *NPA3* support the proposal that Npa3 might play a still to define role in ribosome



biogenesis. Interestingly, *UTP23*, one of the three genes identified as displaying genetic interactions most similar to *NPA3* in our TheCellMap analysis, is directly involved in ribosome biogenesis.

Additionally, we also uncovered a group of genes displaying synthetic negative interactions with *npa3ΔC* that are important for mitochondrial homeostasis. These findings were rather unexpected, as Npa3 is a cytoplasmic protein with no known mitochondrial function. However, it is noteworthy that Npa3 is quickly mobilized from the cytoplasm to mitochondria after TOR inhibition with rapamycin (Chong et al. 2015; Kraus et al. 2017), indicating that Npa3 participates directly in the mitochondrial response to this stress. A mitochondria-related cellular adaptive response that might involve Npa3 is the mitochondrial precursor-overaccumulation stress (mPOS), where *GIS2*, an *npa3ΔC* interacting gene obtained in our study, is one of the major regulators of this recently described pathway of mitochondria-mediated cell death in yeast, previously associated with TOR signaling pathway (Wang and Chen 2015; Seidel and Meierhofer 2017). Furthermore, the analysis of genetic profiles most similar to *NPA3* employing TheCellMap repository revealed *SAM35* among these genes. As Sam35 plays a critical role in protein targeting to the mitochondria, its failure leads to an accumulation of mitochondrial precursor proteins in the cytoplasm, providing further support to a possible role for Npa3 in the cell response to mitochondrial related proteotoxic stress. Another pathway activated by mitochondrial dysfunction is the retrograde signaling response (Komeili et al. 2000), where the transcription of a set of nuclear genes is rapidly induced by damaged mitochondria. Intriguingly, *DLD3*, a classical gene of this response (Chelstowska et al., 1999), was also identified in

our study as a negative interacting gene with *npa3ΔC*. Although our real time PCR experiments did not show any increase in the transcription of *CIT2*, the classical marker of the retrograde response, they did show an increase in *IDH2*, and probably *IDH1*, expression in *npa3ΔC* cells. These results indicate that *npa3ΔC* cells most likely display a mitochondrial adaptation different from the classical retrograde response. Interestingly, in addition to its enzymatic activity in the tricarboxylic acid cycle, Idh1/Idh2 also regulate mitochondrial translation by binding to the 5'-untranslated region of mitochondrial mRNAs (Elzinga et al. 1993). *IDH1//IDH2* disruption leads to several phenotypes that have been attributed to defects in mitochondrial translation in respiratory deficient cells (Grivell 1995). Thus, one interesting possibility is that an increase in *IDH2* expression may compensate for a putative deficiency in mitochondrial translation in *npa3ΔC* cells. This proposal is further supported by the identification of a robust group of negative interacting genes with *npa3ΔC* that possess well-known roles in mitochondrial translation. These genes regulate protein synthesis at several levels, including *MSW1*, that encodes a tryptophanyl t-RNA synthetase; *MRPL37*, which encodes a protein of the mitochondrial large ribosomal subunit; and *RMD9*, that encodes a protein that binds a dodecamer sequence in mitochondrial mRNAs to protect them from degradation (Nouet et al. 2007; Hillen et al. 2021). Finally, the higher sensitivity displayed by *npa3ΔC* cells to ethidium bromide constitutes another experimental evidence in favor of Npa3 playing a critical role in mitochondrial homeostasis. Collectively, these results point to Npa3 playing an important role in molecular processes in the mitochondria or being integrated with a specific mitochondrial function. We expect

that the results obtained from our SGA analyses will provide valuable information to better understand the role that Npa3 plays, direct or indirectly, in several cellular processes critical for mitochondrial function and ribosome biogenesis.

### **Acknowledgements**

We thank the Consejo Nacional de Ciencia y Tecnología for providing doctoral fellowships to support Martín Mora-García. This work was supported by the Consejo Nacional de Ciencia y Tecnología, grant numbers A1-S-21070 (to RSO) and CB-2015/254365 (to AD). We also received support from Universidad Autónoma de San Luis Potosí, grant number C19-FRC-08-03.03 (to RSO).

## References

- Alonso B, Beraud C, Meguellati S, et al (2013) Eukaryotic GPN-loop GTPases paralogs use a dimeric assembly reminiscent of archeal GPN. *Cell Cycle* 12:463–472. <https://doi.org/10.4161/cc.23367>
- Alonso B, Chaussinand G, Armengaud J, Godon C (2011) A role for GPN-loop GTPase yGPN1 in sister chromatid cohesion. *Cell Cycle* 10:1828–1837. <https://doi.org/10.4161/cc.10.11.15763>
- Baganz F, Hayes A, Marren D, et al (1997) Suitability of replacement markers for functional analysis studies in *Saccharomyces cerevisiae*. *Yeast* 13:1563–1573. [https://doi.org/10.1002/\(sici\)1097-0061\(199712\)13:16<1563::aid-yea240>3.0.co;2-6](https://doi.org/10.1002/(sici)1097-0061(199712)13:16<1563::aid-yea240>3.0.co;2-6)
- Baker Brachmann C, Davies A, Cost GJ, et al (1998) Designer Deletion Strains derived from *Saccharomyces cerevisiae* S288C: a Useful set of Strains and Plasmids for PCR-mediated Gene Disruption and Other Applications. *Yeast* 14:115–132
- Berlin V, Styles CA, Fink GR (1990) BIK1, a protein required for microtubule function during mating and mitosis in *Saccharomyces cerevisiae*, colocalizes with tubulin. *J Cell Biol* 111:2573–2586. <https://doi.org/10.1083/jcb.111.6.2573>
- Bhalla P, Vernekar DV, Gilquin B, et al (2019) Interactome of the yeast RNA polymerase III transcription machinery constitutes several chromatin modifiers and regulators of the genes transcribed by RNA polymerase II. *Gene* 702:205–214. <https://doi.org/10.1016/j.gene.2018.12.037>
- Boeke JD, Trueheart J, Natsoulis G, Fink GR (1987) 5-Fluoroorotic acid as a selective agent in yeast molecular genetics. *Methods Enzymol* 154:164–175. [https://doi.org/10.1016/0076-6879\(87\)54076-9](https://doi.org/10.1016/0076-6879(87)54076-9)
- Butow RA, Avadhani NG (2004) Mitochondrial signaling: The retrograde response. *Molecular Cell* 14:1–15. [https://doi.org/10.1016/S1097-2765\(04\)00179-0](https://doi.org/10.1016/S1097-2765(04)00179-0)
- Calera MR, Zamora-Ramos C, Araiza-Villanueva MG, et al (2011) Parcs/Gpn3 is required for the nuclear accumulation of RNA polymerase II. *Biochim Biophys Acta* 1813:1708–1716. <https://doi.org/10.1016/j.bbamcr.2011.07.005>
- Castano I, Kaur R, Pan S, et al (2003) Tn7-based genome-wide random insertional mutagenesis of *Candida glabrata*. *Genome Res* 13:905–915. <https://doi.org/10.1101/gr.848203>
- Chelstowska A, Liu Z, Jia Y, et al (1999) Signalling between mitochondria and the nucleus regulates the expression of a new D-lactate dehydrogenase activity in yeast. *Yeast* 15:1377–1391. [https://doi.org/10.1002/\(SICI\)1097-0061\(19990930\)15:13<1377::AID-YEA473>3.0.CO;2-0](https://doi.org/10.1002/(SICI)1097-0061(19990930)15:13<1377::AID-YEA473>3.0.CO;2-0)

- Chen XJ, Wang X, Kaufman BA, Butow RA (2005) Aconitase couples metabolic regulation to mitochondrial DNA maintenance. *Science* (1979) 307:714–717. <https://doi.org/10.1126/science.1106391>
- Chong YT, Koh JL, Friesen H, et al (2015) Yeast proteome dynamics from single cell imaging and automated analysis. *Cell* 161:1413–1424. <https://doi.org/10.1016/j.cell.2015.04.051>
- Costanzo M, Baryshnikova A, Bellay J, et al (2010) The genetic landscape of a cell. *Science* 327:425–431. <https://doi.org/10.1126/science.1180823>
- Costanzo M, VanderSluis B, Koch EN, et al (2016) A global genetic interaction network maps a wiring diagram of cellular function. *Science* (1979) 353:14. <https://doi.org/10.1126/science.aaf1420>
- Czeko E, Seizl M, Augsberger C, et al (2011) Iwr1 directs RNA Polymerase II nuclear import. *Molecular Cell* 42:261–266. <https://doi.org/10.1016/j.molcel.2011.02.033>
- DeLuna A, Vetsigian K, Shores N, et al (2008) Exposing the fitness contribution of duplicated genes. *Nature Genetics* 40:676–681. <https://doi.org/10.1038/ng.123>
- Deplazes A, Möckli N, Luke B, et al (2009) Yeast Uri1p promotes translation initiation and may provide a link to cotranslational quality control. *Embo J* 28:1429–1441. <https://doi.org/10.1038/emboj.2009.98>
- Dez C, Froment C, Noaillac-Depeyre J, et al (2004) Npa1p, a component of very early pre-60S ribosomal particles, associates with a subset of small nucleolar RNPs required for peptidyl transferase center modification. *Mol Cell Biol* 24:6324–6337. <https://doi.org/10.1128/mcb.24.14.6324-6337.2004>
- Elzinga SDJ, Bednarz AL, van Oosterum K, et al (1993) Yeast mitochondrial NAD (+)-dependent isocitrate dehydrogenase is an RNA-binding protein. *Nucleic Acids Research* 21:5328–5331. <https://doi.org/10.1093/nar/21.23.5328>
- Fehrenbacher KL, Boldogh IR, Pon LA (2005) A role for Jsn1p in recruiting the Arp2/3 complex to mitochondria in budding yeast. *Mol Biol Cell* 16:5094–5102. <https://doi.org/10.1091/mbc.e05-06-0590>
- Fernández-Del-Río L, Kelly ME, Contreras J, et al (2020) Genes and lipids that impact uptake and assimilation of exogenous coenzyme Q in *Saccharomyces cerevisiae*. *Free Radic Biol Med* 154:105–118. <https://doi.org/10.1016/j.freeradbiomed.2020.04.029>
- Field CM, Kellogg D (1999) Septins: cytoskeletal polymers or signalling GTPases? *Trends Cell Biol* 9:387–394. [https://doi.org/10.1016/s0962-8924\(99\)01632-3](https://doi.org/10.1016/s0962-8924(99)01632-3)
- Forget D, Lacombe AA, Cloutier P, et al (2010) The protein interaction network of the human transcription machinery reveals a role for the conserved GTPase RPAP4/GPN1 and

- microtubule assembly in nuclear import and biogenesis of RNA polymerase II. *Mol Cell Proteomics* 9:2827–2839. <https://doi.org/10.1074/mcp.M110.003616>
- Garay E, Campos SE, de La Cruz G, et al (2014) High-resolution profiling of stationary-phase survival reveals yeast longevity factors and their genetic interactions. *PLoS Genet* 10:1004168. <https://doi.org/10.1371/journal.pgen.1004168>
- Gerber AP, Herschlag D, Brown PO (2004) Extensive association of functionally and cytologically related mRNAs with Puf family RNA-binding proteins in yeast. *PLoS Biology* 2:E79. <https://doi.org/10.1371/journal.pbio.0020079>
- Giaever G, Chu AM, Ni L, et al (2002) Functional profiling of the *Saccharomyces cerevisiae* genome. *Nature* 418:387–391. <https://doi.org/10.1038/nature00935>
- Goldring ES, Grossman LI, Krupnick D, et al (1970) The petite mutation in yeast. Loss of mitochondrial deoxyribonucleic acid during induction of petites with ethidium bromide. *J Mol Biol* 52:323–335. [https://doi.org/10.1016/0022-2836\(70\)90033-1](https://doi.org/10.1016/0022-2836(70)90033-1)
- Gorenstein C, Atkinson KD, Falke E v (1978) Isolation and characterization of an actinomycin D-sensitive mutant of *Saccharomyces cerevisiae*
- Grivell LA (1995) Nucleo-mitochondrial interactions in mitochondrial gene expression. *Crit Rev Biochem Mol Biol* 30:121–164. <https://doi.org/10.3109/10409239509085141>
- Grohmann L, Graack HR, Kruff V, et al (1991) Extended N-terminal sequencing of proteins of the large ribosomal subunit from yeast mitochondria. *FEBS Letters* 284:51–56. [https://doi.org/10.1016/0014-5793\(91\)80759-v](https://doi.org/10.1016/0014-5793(91)80759-v)
- Guerrero-Serrano G, Castanedo L, Cristobal-Mondragon GR, et al (2017) Npa3/ScGpn1 carboxy-terminal tail is dispensable for cell viability and RNA polymerase II nuclear targeting but critical for microtubule stability and function. *Biochim Biophys Acta* 1864:451–462. <https://doi.org/10.1016/j.bbamcr.2016.12.010>
- Hibbs MA, Hess DC, Myers CL, et al (2007) Exploring the functional landscape of gene expression: directed search of large microarray compendia. *Bioinformatics* 23:2692–2699. <https://doi.org/10.1093/bioinformatics/btm403>
- Higuchi-Sanabria R, Garcia EJ, Tomoiaga D, et al (2016) Characterization of fluorescent proteins for three- and four-color live-cell imaging in *S. cerevisiae*. *PLoS One*. <https://doi.org/10.1371/journal.pone.0146120>
- Hillen HS, Markov DA, Wojtas ID, et al (2021) The pentatricopeptide repeat protein Rmd9 recognizes the dodecameric element in the 3' -UTRs of yeast mitochondrial mRNAs. *Proc Natl Acad Sci USA* 118:1–8. <https://doi.org/10.1073/pnas.2009329118/-/DCSupplemental>. Published

- Hoareau-Aveilla C, Fayet-Lebaron E, Jády BE, et al (2012) Utp23p is required for dissociation of snR30 small nucleolar RNP from preribosomal particles. *Nucleic Acids Research* 40:3641–3652. <https://doi.org/10.1093/nar/gkr1213>
- Hobbs AEA, Srinivasan M, McCaffery JM, Jensen RE (2001) Mmm1p, a mitochondrial outer membrane protein, is connected to mitochondrial DNA (Mtdna) nucleoids and required for Mtdna stability. *J Cell Biol* 152:401–410. <https://doi.org/10.1083/jcb.152.2.401>
- Hughes TR, Roberts CJ, Dai H, et al (2000) Widespread aneuploidy revealed by DNA microarray expression profiling. *Nature Genetics* 25:333–337. <https://doi.org/10.1038/77116>
- Jorgensen P, Nishikawa JL, Breikreutz B-J, Tyers M (2002) Systematic identification of pathways that couple cell growth and division in yeast. *Science* 297:395–400. <https://doi.org/10.1126/science.1070850>
- Kaboli S, Yamakawa T, Sunada K, et al (2014) Genome-wide mapping of unexplored essential regions in the *Saccharomyces cerevisiae* genome: evidence for hidden synthetic lethal combinations in a genetic interaction network. *Nucleic Acids Res* 42:9838–9853. <https://doi.org/10.1093/nar/gku576>
- Komeili A, Wedaman KP, O’Shea EK, Powers T (2000) Mechanism of metabolic control. Target of rapamycin signaling links nitrogen quality to the activity of the Rtg1 and Rtg3 transcription factors. *J Cell Biol* 151:863–878. <https://doi.org/10.1083/jcb.151.4.863>
- Kraus OZ, Grys BT, Ba J, et al (2017) Automated analysis of high-content microscopy data with deep learning. *Mol syst biol* 13:924. <https://doi.org/10.15252/msb.20177551>
- Krogan NJ, Cagney G, Yu H, et al (2006) Global landscape of protein complexes in the yeast *Saccharomyces cerevisiae*. *Nature* 440:637–643. <https://doi.org/10.1038/nature04670>
- Lacombe AA, Forget D, Cloutier P, et al (2010) Nuclear import of RNA polymerase II requires the conserved GPN-loop GTPase XAB1/GPN1. *Faseb Journal* 24:1
- Lapointe CP, Preston MA, Wilinski D, et al (2017) Architecture and dynamics of overlapped RNA regulatory networks. *RNA* 23:1636–1647. <https://doi.org/10.1261/rna.062687.117>
- Leipe DD, Wolf YI, Koonin E v, Aravind L (2002) Classification and evolution of P-loop GTPases and related ATPases. *J Mol Biol* 317:41–72. <https://doi.org/10.1006/jmbi.2001.5378>
- Liu X, Xie D, Hua Y, et al (2020) Npa3 interacts with Gpn3 and assembly factor Rba50 for RNA polymerase II biogenesis. *Faseb J*. <https://doi.org/10.1096/fj.202001523R>
- Liu Z, Butow RA (2006) Mitochondrial retrograde signaling. *Annu Rev Genet* 40:159–185. <https://doi.org/10.1146/annurev.genet.40.110405.090613>

- Luévano-Martínez LA, Forni MF, dos Santos VT, et al (2015) Cardiolipin is a key determinant for mtDNA stability and segregation during mitochondrial stress. *Biochim Biophys Acta - Bioenerg* 1847:587–598. <https://doi.org/10.1016/J.BBABIO.2015.03.007>
- Maity S, Chakrabarti O (2021) Mitochondrial protein import as a quality control sensor. *Biol Cell* 113:375–400
- Martínez-Fernández V, Cuevas-Bermúdez A, Gutiérrez-Santiago F, et al (2020) Prefoldin-like Bud27 influences the transcription of ribosomal components and ribosome biogenesis in *Saccharomyces cerevisiae*. *RNA*. <https://doi.org/10.1261/rna.075507.120>
- Milenkovic D, Kozjak V, Wiedemann N, et al (2004) Sam35 of the mitochondrial protein sorting and assembly machinery is a peripheral outer membrane protein essential for cell viability. *J Biol Chem* 279:22781–22785. <https://doi.org/10.1074/jbc.C400120200>
- Minaker SW, Filiatrault MC, Ben-Aroya S, et al (2013) Biogenesis of RNA Polymerases II and III requires the conserved GPN small GTPases in *Saccharomyces cerevisiae*. *Genetics* 193:853-U305. <https://doi.org/10.1534/genetics.112.148726>
- Miron-Garcia MC, Garrido-Godino AI, Garcia-Molinero V, et al (2013) The prefoldin bud27 mediates the assembly of the eukaryotic RNA polymerases in an rpb5-dependent manner. *PLoS Genet* 9:e1003297. <https://doi.org/10.1371/journal.pgen.1003297>
- Myers AM, Tzagoloff A (1985) MSW, a yeast gene coding for mitochondrial tryptophanyl-tRNA synthetase. *J Biol Chem* 260:15371–15377. [https://doi.org/10.1016/s0021-9258\(18\)95746-7](https://doi.org/10.1016/s0021-9258(18)95746-7)
- Niesser J, Wagner FR, Kostrewa D, et al (2016) Structure of GPN-Loop GTPase Npa3 and implications for RNA Polymerase II assembly. *Mol Cell Biol* 36:820–831. <https://doi.org/10.1128/mcb.01009-15>
- Nouet C, Bourens M, Hlavacek O, et al (2007) Rmd9p controls the processing/stability of mitochondrial mRNAs and its overexpression compensates for a partial deficiency of oxa1p in *Saccharomyces cerevisiae*. *Genetics* 175:1105–1115. <https://doi.org/10.1534/genetics.106.063883>
- Paschen SA, Neupert W, Rapaport D (2005) Biogenesis of beta-barrel membrane proteins of mitochondria. *Trends Biochem Sci* 30:575–582. <https://doi.org/10.1016/j.tibs.2005.08.009>
- Perry RP, Kelley DE (1970) Inhibition of RNA synthesis by actinomycin D: Characteristic dose-response of different RNA species. *J Cell Physiol* 76:127–139. <https://doi.org/10.1002/jcp.1040760202>
- Phillips PC (2008) Epistasis-the essential role of gene interactions in the structure and evolution of genetic systems. *Nat Rev Genet* 9:855–867. <https://doi.org/10.1038/nrg2452>



- Raudvere U, Kolberg L, Kuzmin I, et al (2019) g:Profiler: a web server for functional enrichment analysis and conversions of gene lists (2019 update). *Nucleic Acids Research* 47:W191–W198. <https://doi.org/10.1093/nar/gkz369>
- Roguev A, Wiren M, Weissman JS, Krogan NJ (2007) High-throughput genetic interaction mapping in the fission yeast *Schizosaccharomyces pombe*. *Nature Methods* 4:861–866. <https://doi.org/10.1038/nmeth1098>
- Scherrer T, Femmer C, Schiess R, et al (2011) Defining potentially conserved RNA regulons of homologous zinc-finger RNA-binding proteins. *Genome Biol* 12:R3. <https://doi.org/10.1186/gb-2011-12-1-r3>
- Schlitt T, Palin K, Rung J, et al (2003) From gene networks to gene function. *Genome Res* 13:2568–2576. <https://doi.org/10.1101/gr.1111403>
- Schmitt ME, Brown TA, Truempower BL (1990) A rapid and simple method for preparation of RNA from *Saccharomyces cerevisiae*. *Nucleic Acids Research* 18:3091–3092. <https://doi.org/10.1093/nar/18.10.3091>
- Seidel G, Meierhofer D (2017) Quantitative global proteomics of yeast PBP1 deletion mutants and their stress responses identifies glucose metabolism, mitochondrial, and stress granule changes. *J Proteome Res* 16:504–515. <https://doi.org/10.1021/acs.jproteome.6b00647>
- Shannon P, Markiel A, Ozier O, et al (2003) Cytoscape: a software environment for integrated models of biomolecular interaction networks. *Genome Research* 13:2498–2504. <https://doi.org/10.1101/gr.1239303>
- Sliwa P, Korona R (2005) Loss of dispensable genes is not adaptive in yeast. *Proc Natl Acad Sci U S A* 102:17670–17674. <https://doi.org/10.1073/pnas.0505517102>
- Steff A-M, Ne Fortin M, Arguin C, Hugo P (2001) Detection of a decrease in green fluorescent protein fluorescence for the monitoring of cell death: An assay amenable to high-throughput screening technologies. *Cytometry*. <https://doi.org/10.1002/cyto.10024>
- Stenger M, Le DT, Klecker T, Westermann B (2020) Systematic analysis of nuclear gene function in respiratory growth and expression of the mitochondrial genome in *Saccharomyces cerevisiae*. *Microb Cell* 7:234–249. <https://doi.org/10.15698/mic2020.09.729>
- Talavera D, Robertson DL, Lovell SC (2013) The role of protein interactions in mediating essentiality and synthetic lethality. *PLoS One* 8:e62866. <https://doi.org/10.1371/journal.pone.0062866>
- Tong AH, Boone C (2006) Synthetic genetic array analysis in *Saccharomyces cerevisiae*. *Methods Mol Biol* 313:171–192. <https://doi.org/10.1385/1-59259-958-3:171>

- Tong AH, Evangelista M, Parsons AB, et al (2001) Systematic genetic analysis with ordered arrays of yeast deletion mutants. *Science* (1979) 294:2364–2368. <https://doi.org/10.1126/science.1065810>
- Usaj M, Tan Y, Wang W, et al (2017) TheCellMap.org: A Web-accessible database for visualizing and mining the global yeast genetic interaction network. *G3* 7:1539–1549. <https://doi.org/10.1534/g3.117.040220>
- van Welsem T, Frederiks F, Verzijlbergen KF, et al (2008) Synthetic lethal screens identify gene silencing processes in yeast and implicate the acetylated amino terminus of Sir3 in recognition of the nucleosome core. *Mol Cell Biol* 28:3861–3872. <https://doi.org/10.1128/mcb.02050-07>
- Vernekar DV, Bhargava P (2015) Yeast Bud27 modulates the biogenesis of Rpc128 and Rpc160 subunits and the assembly of RNA polymerase III. *Biochim Biophys Acta - Gene Regul Mech* 1849:1340–1353. <https://doi.org/10.1016/j.bbagr.2015.09.010>
- Wang X, Chen XJ (2015) A cytosolic network suppressing mitochondria-mediated proteostatic stress and cell death. *Nature* 524:481–484. <https://doi.org/10.1038/nature14859>
- Wickens M, Bernstein DS, Kimble J, Parker R (2002) A PUF family portrait: 3'UTR regulation as a way of life. *Trends Genet* 18:150–157. [https://doi.org/10.1016/s0168-9525\(01\)02616-6](https://doi.org/10.1016/s0168-9525(01)02616-6)
- Winzler EA, Shoemaker DD, Astromoff A, et al (1999) Functional characterization of the *Saccharomyces cerevisiae* genome by gene deletion and parallel analysis. *Science* (1979) 285:901–906. <https://doi.org/10.1126/science.285.5429.901>
- Wittinghofer A, Vetter IR (2011) Structure-function relationships of the G domain, a canonical switch motif. *Annu Rev Biochem* 80:943–971. <https://doi.org/10.1146/annurev-biochem-062708-134043>
- Yanez-Carrillo P, Orta-Zavalza E, Gutierrez-Escobedo G, et al (2015) Expression vectors for C-terminal fusions with fluorescent proteins and epitope tags in *Candida glabrata*. *Fungal Genet Biol* 80:43–52. <https://doi.org/10.1016/j.fgb.2015.04.020>
- Yuan DS, Stearman R, Dancis A, et al (1995) The Menkes/Wilson disease gene homologue in yeast provides copper to a ceruloplasmin-like oxidase required for iron uptake. *Proc Natl Acad Sci USA* 92:2632–2636. <https://doi.org/10.1073/pnas.92.7.2632>
- Zeng FL, Hua Y, Liu XQ, et al (2018) Gpn2 and Rba50 directly participate in the assembly of the Rpb3 subcomplex in the biogenesis of RNA Polymerase II. *Mol Cell Biol* 38:11. <https://doi.org/10.1128/mcb.00091-18>

## Figure legends

**Figure 1.** Generation of *S. cerevisiae* MCR03 and Mc $\Delta$ 01 query strains. **A)** MCR03 and Mc $\Delta$ 01 strains were generated in the YEG01 genetic background which expresses constitutively the red fluorescence protein mCherry from the *PDC1* locus in chromosome XII. The NATr cassette (CTA1<sub>3'UTR</sub>-TEF1<sub>5'UTR</sub>-*natMX4*-TEF1<sub>3'UTR</sub>) was integrated in chromosome X at the *NPA3* locus, after the ORF sequence of *NPA3* gene. The disruption of *NPA3* C-terminal extension coding region was accomplished by the integration of the NATr cassette. **B)** Mc $\Delta$ 01 and MCR03 strains displayed a proliferation rate indistinguishable from the parental strain *YEG01-RFP*. Cells were inoculated in YPD at an OD<sub>600nm</sub> of 0.1 and cell growth was followed over time. The growth assay was performed in a Bioscreen C analyzer in honeycomb plates using a volume of 300  $\mu$ L. OD<sub>600nm</sub> was automatically recorded every 15 min during 24 h (n = 8).

**Figure 2.** Distribution of normalized fluorescence values of single-mutant selection step (KanR) and double-mutant selection step (KanR NatR). Dotted line indicates the detection threshold value (-1.5) for colony growth.

**Figure 3.** Scatter plot with genome-wide screening threshold. Distribution within red dotted line represents array positions with colony growth in single-mutant selection step but no growth in double-mutant selection step. The blue color to yellow color gradient indicates the density of normalized fluorescence value distribution of the array positions.

**Figure 4.** Schematic representation of the SGA coupled to bulk-fluorescence methodology. The SGA starting strain MAT $\alpha$  Mc $\Delta$ 01 (*npa3 $\Delta$ C-NATr*), which expresses constitutively the mCherry red fluorescent protein (RFP-*hphMX4*), was crossed with geneticin (G418) resistant MAT $\alpha$  (*xxx $\Delta$ ::kanMX4*) nonessential gene-deletion collection mutants. After mating, the heterozygous diploids were sporulated, followed by consecutive haploid selection in hygromycin B containing media. The resulting MAT $\alpha$  meiotic progenies were replicated on G418 and hygromycin B containing media, for the selection of nonessential mutation (KanR selection) and RFP, respectively. Thereafter colonies were replicated on G418/clonNAT/hygromycin B containing media for the selection of *xxx $\Delta$ /npa3 $\Delta$ C* double mutant cells (KanR NatR selection) and RFP, respectively. Red fluorescence signal reading was performed at KanR selection step and KanR NatR selection step, and then used to generate a genetic interaction score (GIS).

**Figure 5.** Boxplot of genetic interaction score (GIS) values for each *xxx $\Delta$ /npa3 $\Delta$ C* deletion mutant pair of the high-resolution analysis. Red color indicates reference *HO* double-mutants. Purple color indicates the positive control genes closest to the *NPA3* locus in the chromosome. Gray dotted lines indicate the “stringent cut-off” set on GIS  $\leq -0.42$  value and a more relaxed “lenient cut-off” set on GIS  $\leq -0.2$  value. *p*-value used for t-test: \**p*  $\leq 0.05$ .

**Figure 6.** The *npa3 $\Delta$ C* allele is synthetic lethal with *bud27 $\Delta$* . A) Schematic representation of the plasmid shuffling strategy to evaluate the synthetic negative interaction between *npa3 $\Delta$ C* and *bud27 $\Delta$* . The red arrow represents the random loss

of the *NPA3-URA3* maintenance plasmid during cell division. B) Double chromosomal mutant *npa3Δ/bud27Δ*, carrying an *NPA3-URA3* plasmid together with either an *NPA3-LEU2* plasmid (up) or an *npa3ΔC-LEU2* plasmid (bottom) were grown as described in Materials and Methods. Thereafter, cells were plated onto SCM-Leu or SCM+5-FOA plates, the appropriate combination of nutrients to counter-select for the loss of *NPA3-URA3*, and incubated for 3 days at 30 °C. *bud27Δ* cells formed colonies in the presence of 5-FOA only if they end up carrying the *NPA3-LEU2* but never the *npa3ΔC-LEU2* plasmid, indicating that cells expressing *npa3ΔC-LEU2* and having the *bud27Δ* mutation cannot survive.

**Figure 7.** Network representation of functional enrichment analysis of the 15 synthetic negative interactors with *npa3ΔC*, the top 123 co-expressed genes with *npa3ΔC* synthetic negative interactors and *NPA3*. The enrichment analysis was done as a random query, with an statistical domain scope of only annotated genes and the significance threshold of 0.05, using the g:SCS algorithm. Node Cutoff, FDR  $\leq 0.05$  (biological process GO Term); and Edge Cutoff for similarity coefficient (genes overlapped)  $\leq 0.68$ . Clusters represented with red and green colors were generated by clusterMaker2 plugin with the MCL algorithm. Node size in gray indicates the number of genes within the node.

**Figure 8.** *NPA3* profile similarity subnetwork (modified from TheCellMap). Node's colors indicate the gene annotations from studies considered for global network in TheCellMap. Edges represent the Pearson's correlation coefficients for genetic

interactions profiles similar to *NPA3*: *SAM35* = 0.290, *UTP23* = 0.235, and *CDC10* = 0.206.

**Figure 9.** *npa3ΔC* yeast cells growth display an increased sensitivity to actinomycin D and ethidium bromide. *npa3Δ* yeast cells episomally expressing *Npa3* wt or *npa3ΔC* from the indicated plasmids were spotted onto YPD plates containing: A) no drug or 15 μM actinomycin D (ActD), and B) no drug or 24 μg/mL ethidium bromide (Et. bromide). Plates were incubated for 3 days at 30 °C. In all conditions n=3 but only a representative result is shown.

**Figure 10.** mRNA levels of the retrograde response markers *CIT2*, *IDH1* and *IDH2* in *NPA3* and *npa3ΔC* cells. Expression levels of the indicated genes were determined by real time PCR, as described in Materials and Methods. Blue, green and red columns represent mRNA expression of *CIT2*, *IDH1* and *IDH2*, respectively, in *NPA3* and *npa3ΔC* cells grown in glucose containing media. Two-way ANOVA followed by Tukey's multiple comparisons test was performed. Significant difference in expression levels are indicated: \*\* p<0.05 and \*\*\* p<0.005. n=6.

# Figures

Figure 1

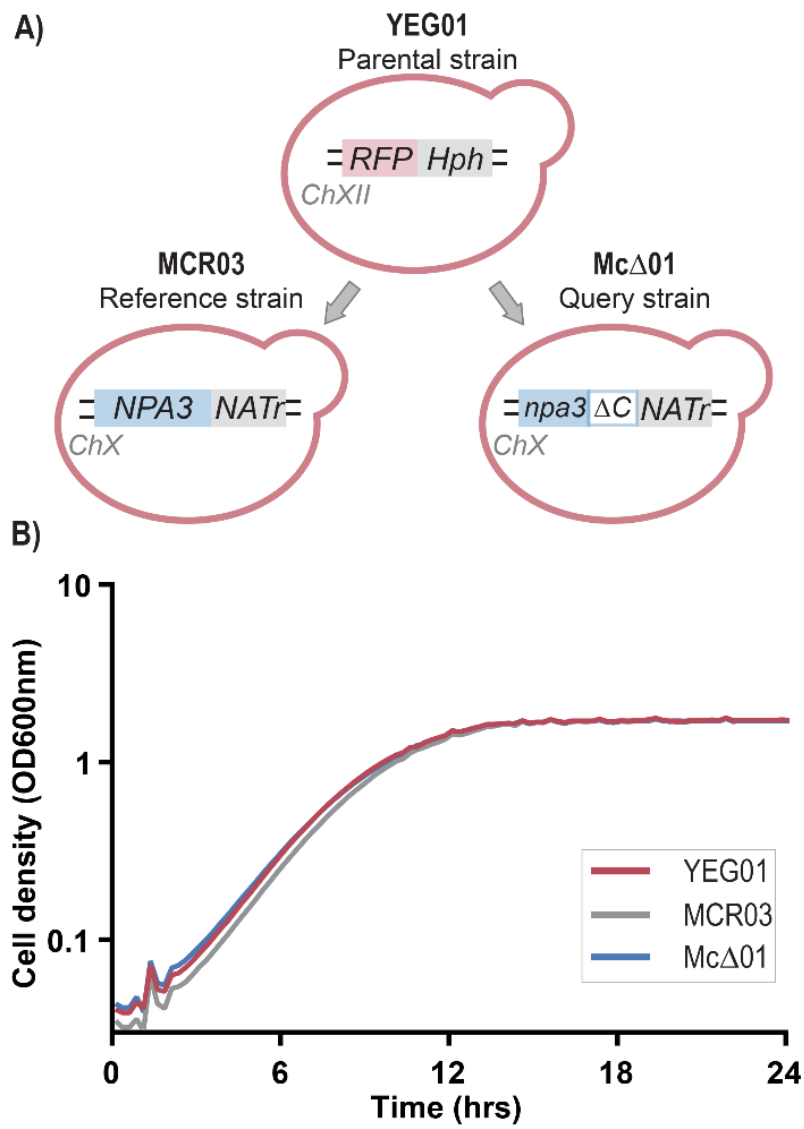


Figure 2

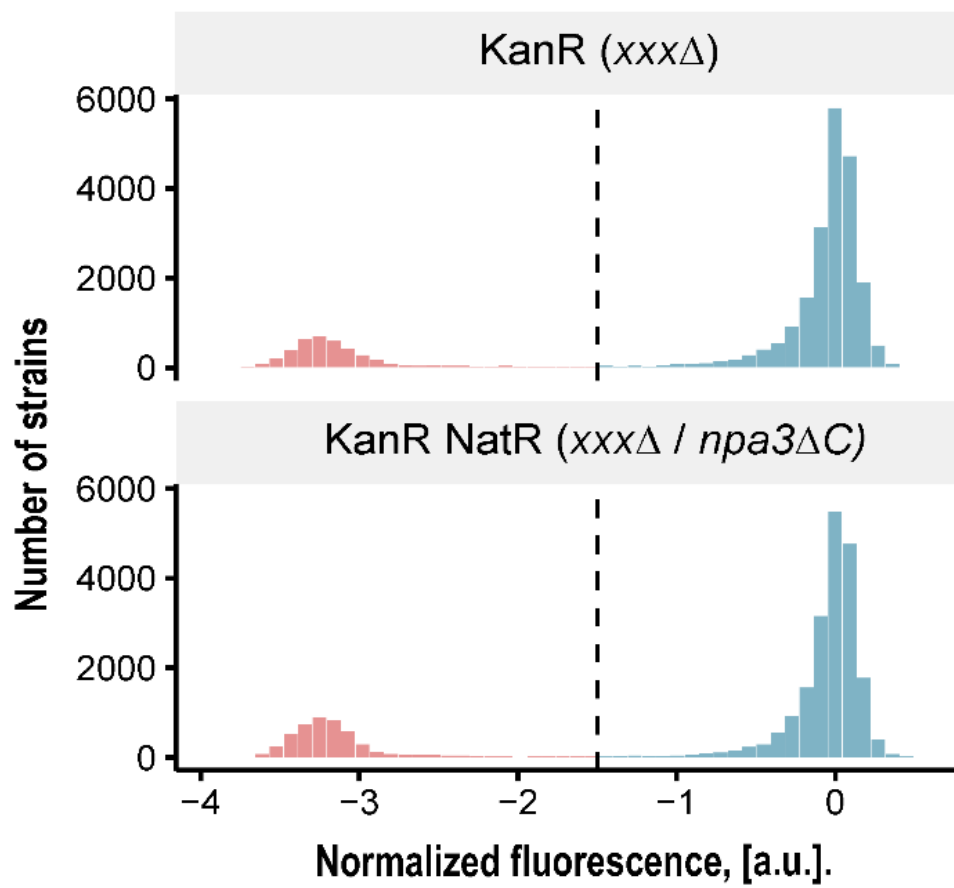




Figure 3

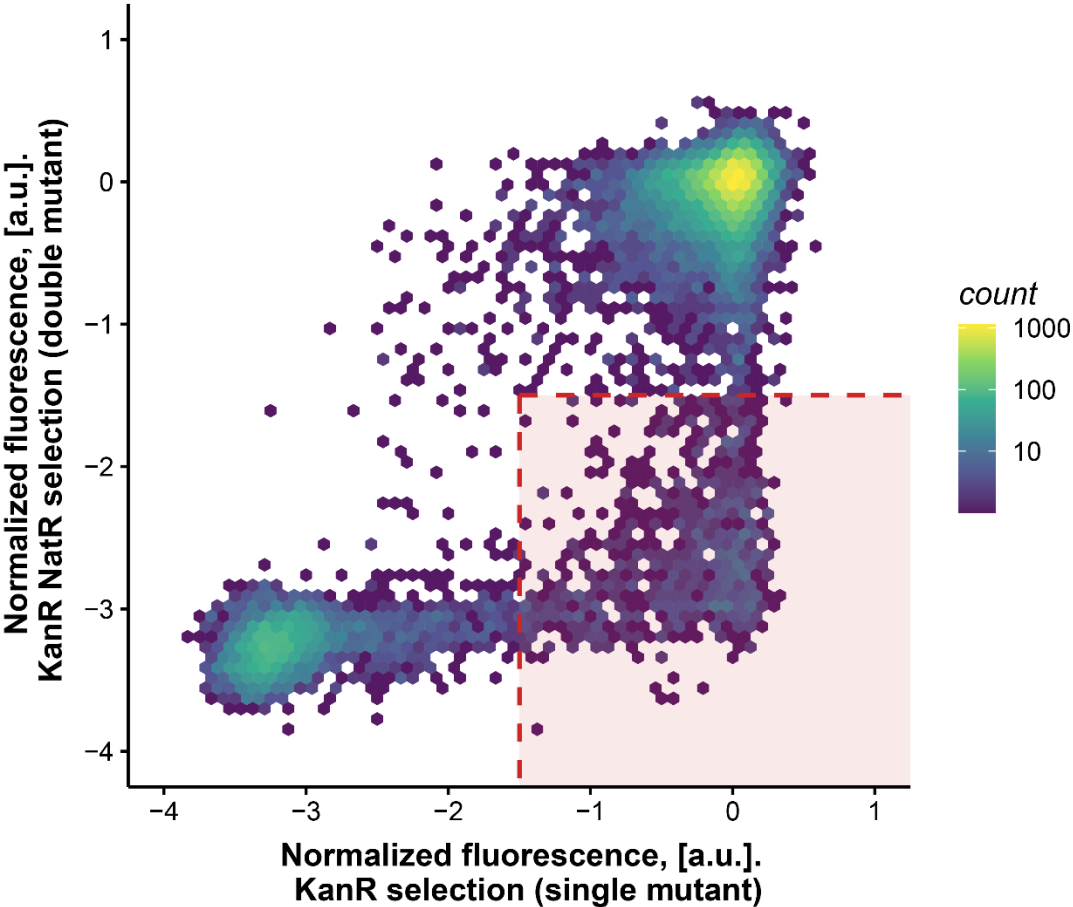


Figure 4

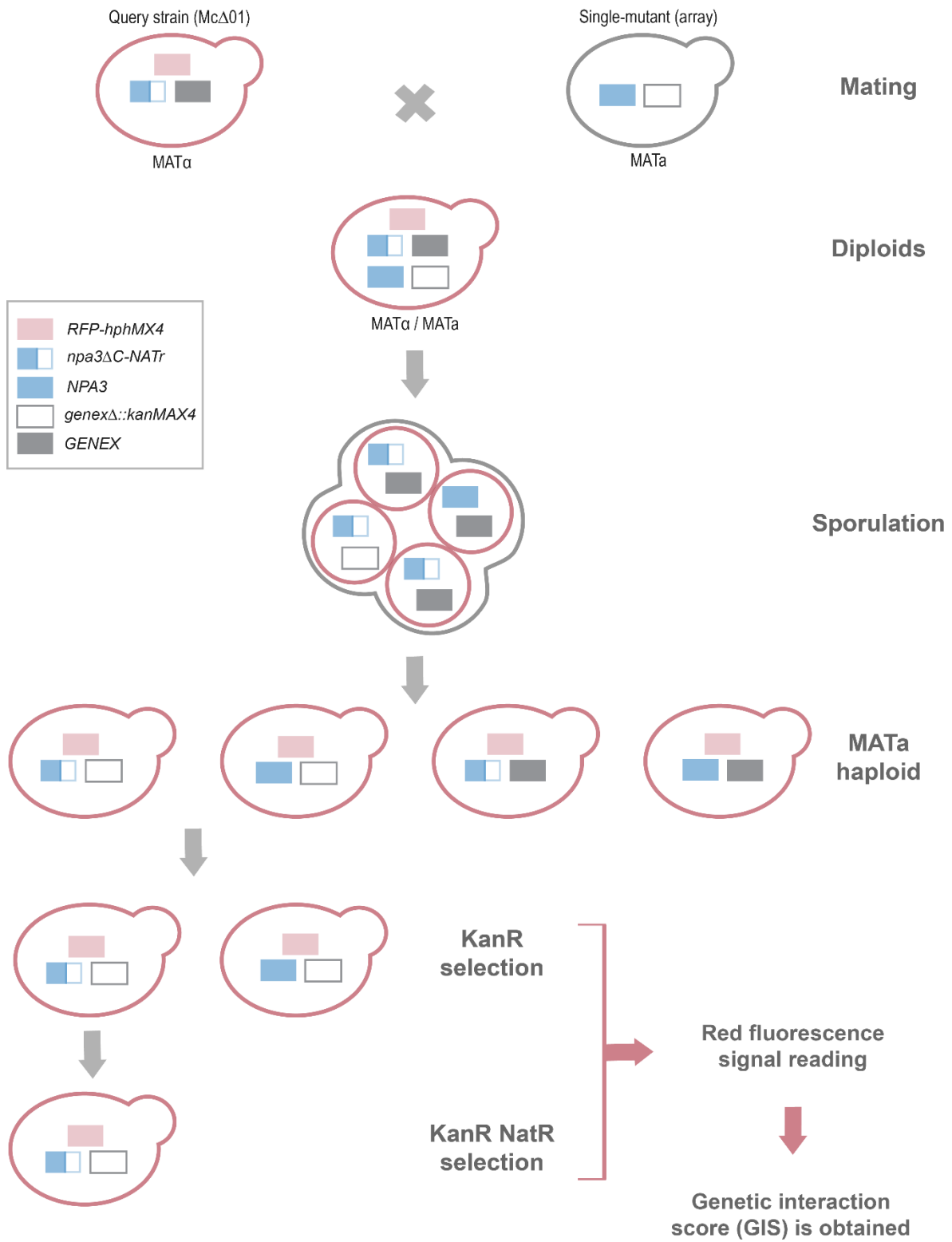


Figure 5

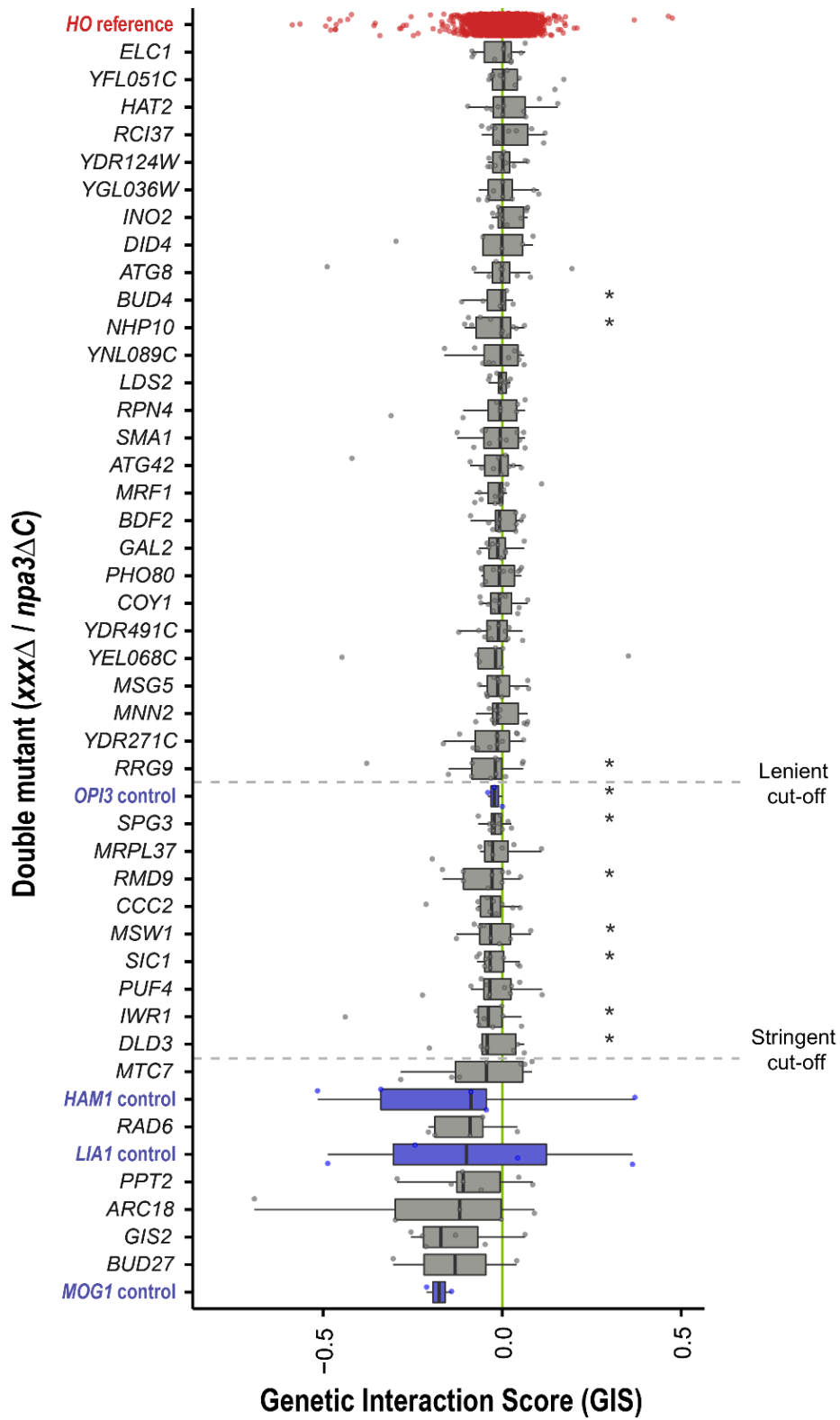


Figure 6

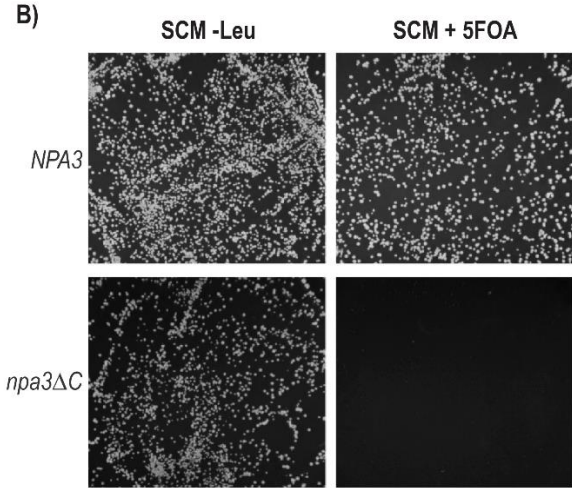
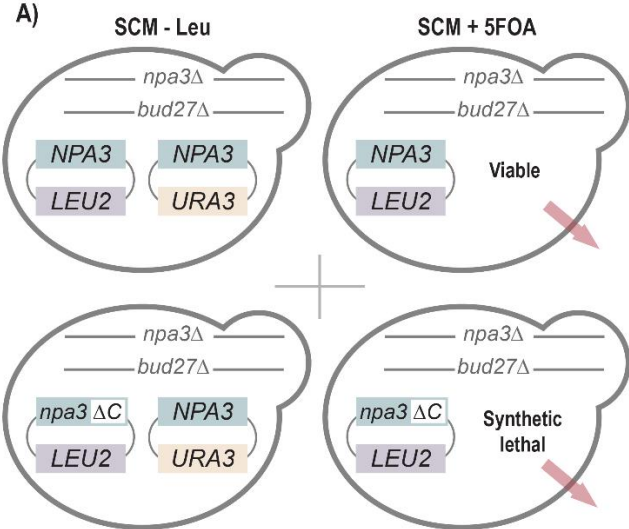


Figure 7

Node size  
(genes)

3310

284

175

62

10

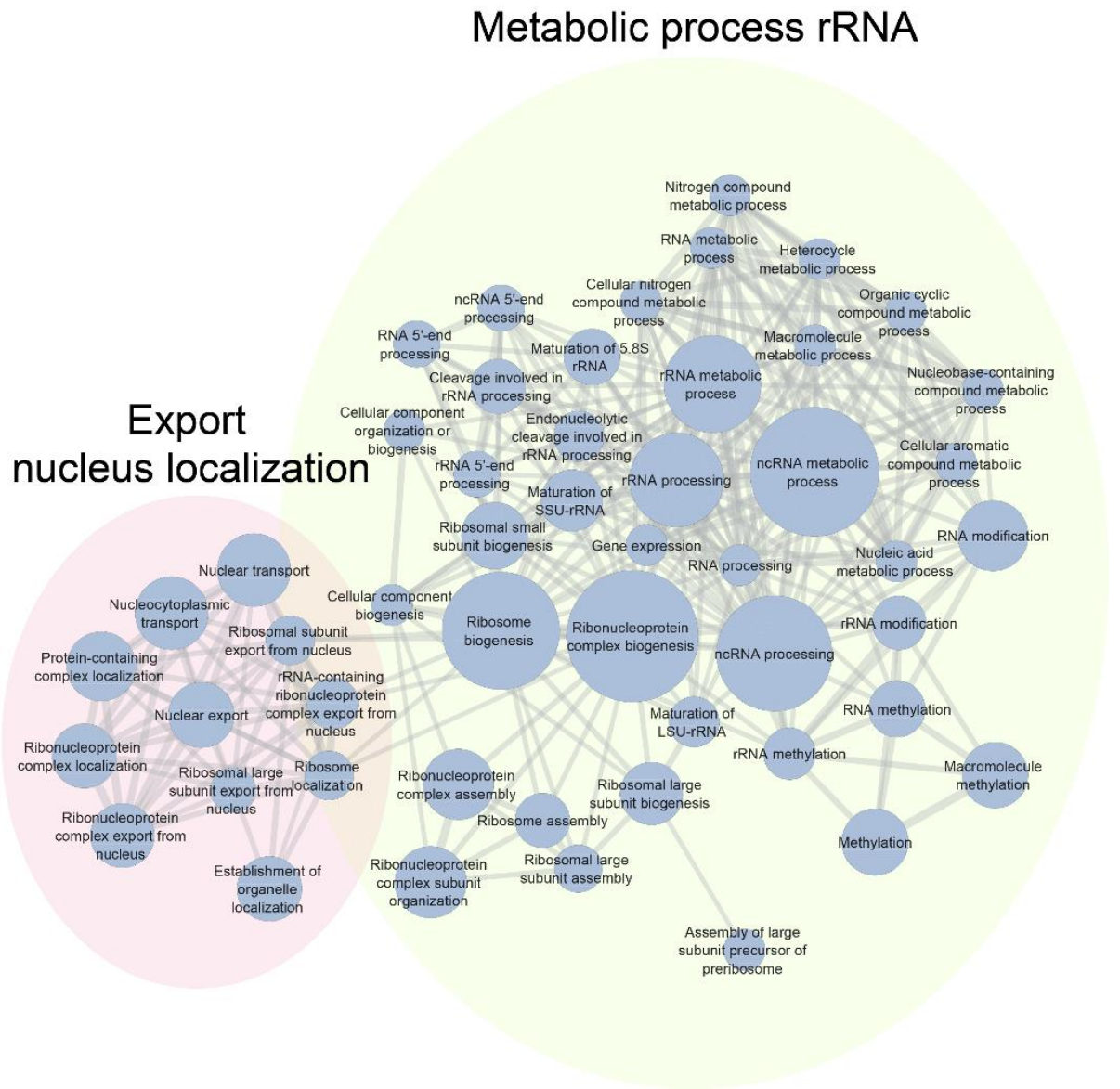


**Figure 8**

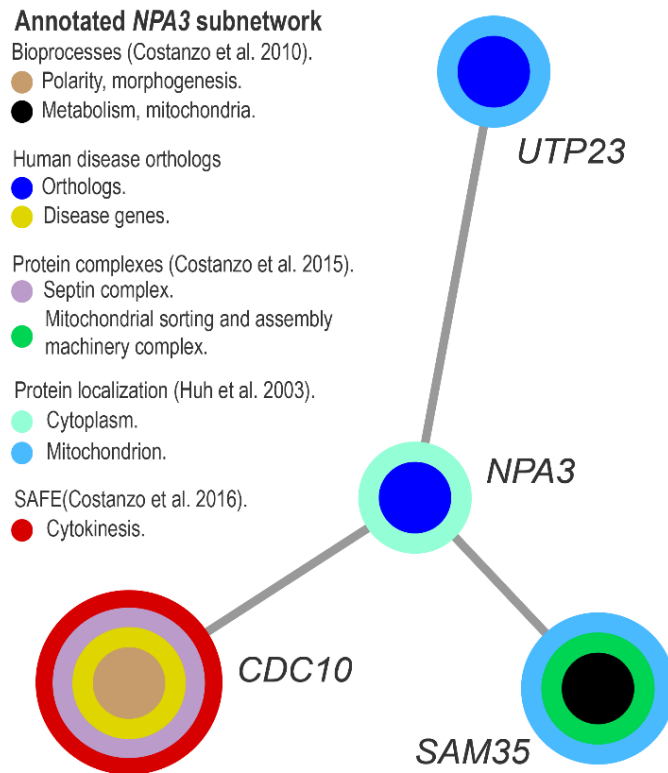


**Figure 9**

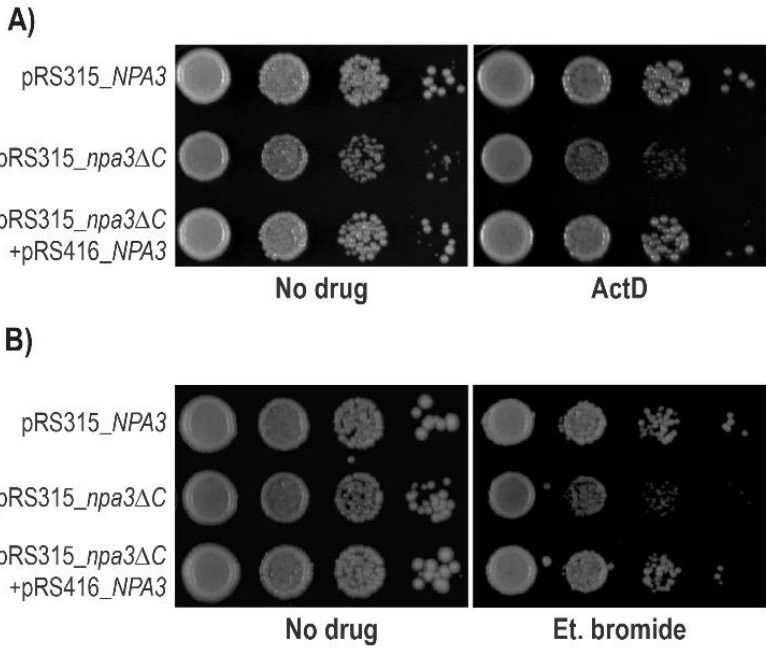
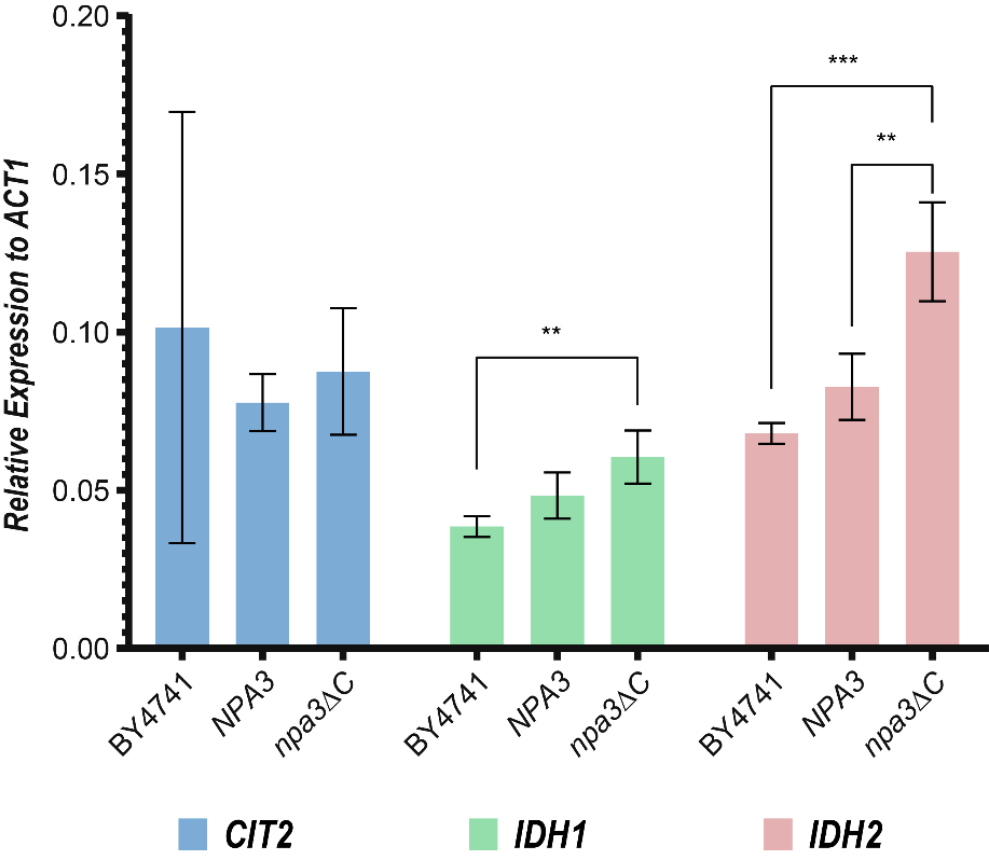


Figure 10





**Table 1** Yeast strains used in this study.

Strain	Genotype	Reference or source
YEG01-RFP	<i>MAT<math>\alpha</math> Pdc1-mCherry-Hyg his3<math>\Delta</math>1, leu2<math>\Delta</math>0, ura3<math>\Delta</math>0, Can1<math>\Delta</math>::Ste2pr(a)_sp_his5, lyp1<math>\Delta</math>::direct repeat</i>	(Garay et al. 2014)
Mc $\Delta$ 01	<i>MAT<math>\alpha</math> Pdc1-mCherry-Hyg his3<math>\Delta</math>1, leu2<math>\Delta</math>0, ura3<math>\Delta</math>0, Can1<math>\Delta</math>::Ste2pr(a)_sp_his5, lyp1<math>\Delta</math>::direct repeat, npa3<math>\Delta</math>C::CTA1t-AgTEFp-natMX4-AgTEFt-NPA3t</i>	This study
MCR03	<i>MAT<math>\alpha</math> Pdc1-mCherry-Hyg his3<math>\Delta</math>1, leu2<math>\Delta</math>0, ura3<math>\Delta</math>0, Can1<math>\Delta</math>::Ste2pr(a)_sp_his5, lyp1<math>\Delta</math>::direct repeat, NPA3-CTA1t-AgTEFp-natMX4-AgTEFt-NPA3t</i>	This study
BY4741	<i>MAT<math>\alpha</math> his3<math>\Delta</math>1, leu2<math>\Delta</math>0, ura3<math>\Delta</math>0, met15<math>\Delta</math>0</i>	(Baker Brachmann et al. 1998)
BYMG20	<i>MAT<math>\alpha</math> his3<math>\Delta</math>1, leu2<math>\Delta</math>0, ura3<math>\Delta</math>0, met15<math>\Delta</math>0, npa3<math>\Delta</math>::natMX4, pRS315-NPA3_LEU2</i>	This study
BYMG21	<i>MAT<math>\alpha</math> his3<math>\Delta</math>1, leu2<math>\Delta</math>0, ura3<math>\Delta</math>0, met15<math>\Delta</math>0, npa3<math>\Delta</math>::natMX4, pRS315-npa3<math>\Delta</math>C_LEU2</i>	This study
BYMG34	<i>MAT<math>\alpha</math> his3<math>\Delta</math>1, leu2<math>\Delta</math>0, ura3<math>\Delta</math>0, met15<math>\Delta</math>0, npa3<math>\Delta</math>::natMX4, pRS315-npa3<math>\Delta</math>C_LEU2, pRS416-NPA3_URA3</i>	This study
BYMG56	<i>MAT<math>\alpha</math> his3<math>\Delta</math>1, leu2<math>\Delta</math>0, ura3<math>\Delta</math>0, met15<math>\Delta</math>0, npa3<math>\Delta</math>:: natMX4, bud27<math>\Delta</math>::kanMX4, pRS416-NPA3_URA3, pRS315-NPA3_LEU2</i>	This study
BYMG57	<i>MAT<math>\alpha</math> his3<math>\Delta</math>1, leu2<math>\Delta</math>0, ura3<math>\Delta</math>0, met15<math>\Delta</math>0, npa3<math>\Delta</math>:: natMX4, bud27<math>\Delta</math>::kanMX4, pRS416-NPA3_URA3, pRS315-npa3<math>\Delta</math>C_LEU2</i>	This study

**Table 2** Primers used in this study.

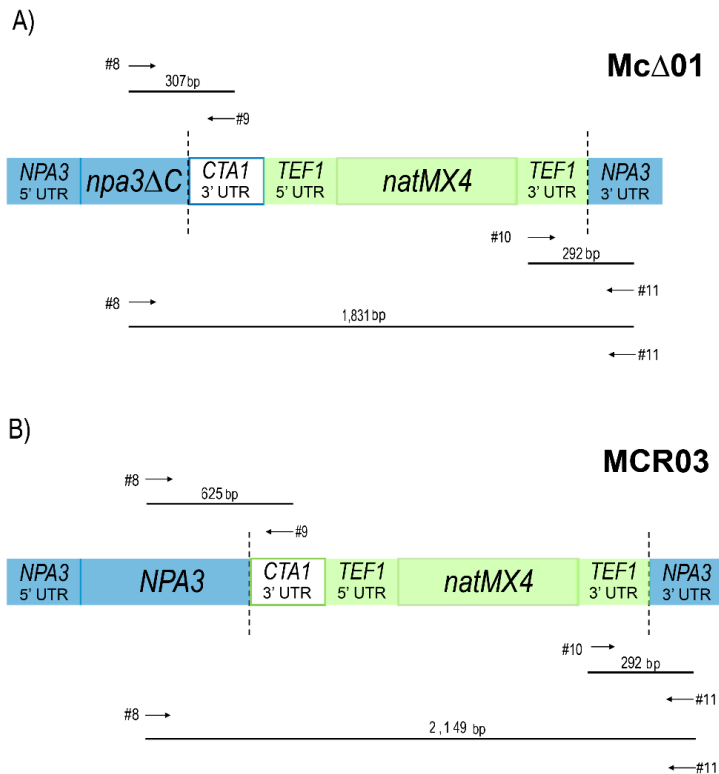
No.	Sequence (5'-3')
3	CAAGAACGTGAAAAAGCATTGAACCTAAAAAAGAAAAAGGAAGAGTAAGTGCGC TTTTGAACCACGTAAG
4	CTGCGGGTCGAATGATCGCCGAACCAAAGGACTATACGTAGTTATCGACACTGG ATGGCGGCGT
8	CTATTCCCAGCTAGACGTCGTG
9	GCTAGCGCTTTGAACTGAACTATTG
10	TTCGCCTCGACATCATCTGC
11	GTTTCTCACTGCATTCTACAGGG
32	CTGCGGGTCGAATGATCGCCGAACCAAAGGACTATACGTAGTTATCGACACTGG ATGGCGGCGTT
84	TAGCGCACACAAACAACACTACAAAACGCAATAACGACACAGCAAGATAGAGATCC GCTTGCCTCGTCCCCG
89	ATATTCTGTAGAATTTTATAGTAAACAGGTATCCTCAGACTGTAATAGCCGACAT GGAGGCCCAGAATAC
90	ATACGTATATGTTAATATAGATTCTGATTTACTTTCTGTCTCCATATGGGCAGTAT AGCGACCAGCATTTC
105	GTTTCATTTGATGCTCGATGAG
106	GAAACGTGAGTCTTTTCCTTAC
123	CAAGCTTTGTATATGTCTATGCC
124	CAGTATCATCCAAAGTAGTAGAC
125	GTATGAGAGGTATTCCAGGGAGC
126	CTTCTGGTAGTGGTTGTGAGCTTC
127	GGTGACGGTGTGGGAAAGAAATC
128	GACGCCTTCCTTATGATCTGTTTGC
129	GTTTCGTCCCGCAAAGTCTATTGAAG
130	GAACAACGCCAGGGCAAACCTATG
131	AGTTGCCCCAGAAGAACACC
132	CGTAGAAGGCTGGAACGTTGA

**Table 3** Putative negative genetic interactions identified in the *npa3ΔC* genome-wide screening.

Putative hits with biological known function				Putative hits with biological unknown function
<i>ARC18</i>	<i>GAL2</i>	<i>PUF4</i>	<i>WHI5</i>	<i>ECM18</i>
<i>ATG2</i>	<i>GIS2</i>	<i>RAD33</i>		<i>MTC7</i>
<i>ATG42</i>	<i>GSH1</i>	<i>RAD6</i>		<i>RCI37</i>
<i>ATG8</i>	<i>HAT2</i>	<i>RHO2</i>		<i>RTC4</i>
<i>BDF2</i>	<i>INO2</i>	<i>RIM15</i>		<i>SDD1</i>
<i>BUD27</i>	<i>IZH1</i>	<i>RMD9</i>		<i>SPG3</i>
<i>BUD4</i>	<i>LDS2</i>	<i>RPN4</i>		<i>SRL2</i>
<i>CAF4</i>	<i>LEU9</i>	<i>RRG9</i>		<i>YDR124W</i>
<i>CCC2</i>	<i>MGA2</i>	<i>RTS1</i>		<i>YDR094W</i>
<i>CNL1</i>	<i>MIS1</i>	<i>SDD2</i>		<i>YDR491C</i>
<i>COY1</i>	<i>MNN2</i>	<i>SHU2</i>		<i>YDL071C</i>
<i>CUR1</i>	<i>MON2</i>	<i>SIC1</i>		<i>YDR271C</i>
<i>CUS2</i>	<i>MRF1</i>	<i>SMA1</i>		<i>YEL067C</i>
<i>DAL81</i>	<i>MRPL37</i>	<i>SPF1</i>		<i>YEL068C</i>
<i>DID4</i>	<i>MSG5</i>	<i>STO1</i>		<i>YFL051C</i>
<i>DLD3</i>	<i>MSW1</i>	<i>SWC5</i>		<i>YGL036W</i>
<i>DNF2</i>	<i>NHP10</i>	<i>TEX1</i>		<i>NRS1</i>
<i>DNL4</i>	<i>PHO80</i>	<i>TPS3</i>		<i>YML012C-A</i>
<i>ELC1</i>	<i>PHO90</i>	<i>UBX2</i>		<i>YNL089C</i>
<i>ERG3</i>	<i>PPA2</i>	<i>VAC8</i>		
<i>FRD1</i>	<i>PPT2</i>	<i>VPS64</i>		

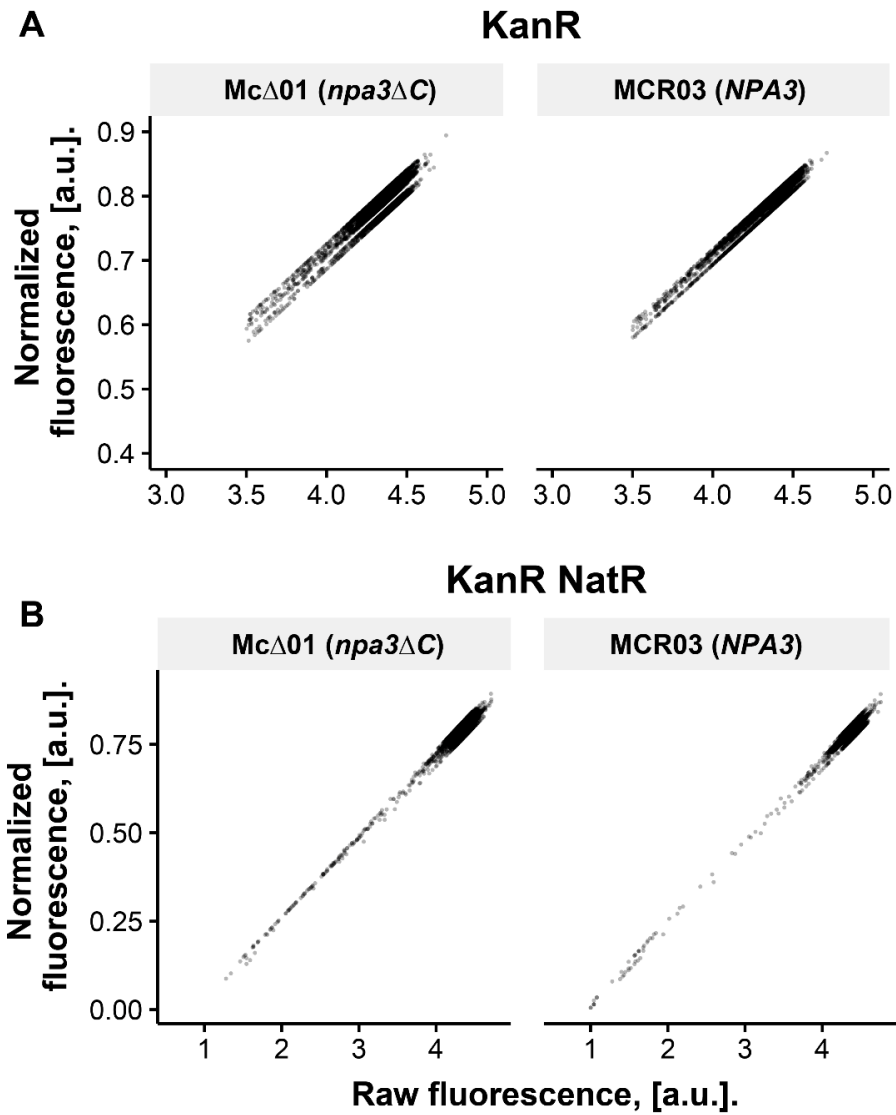
## Supplemental Material

### Supplemental Figure 1



PCR strategy to test genomic DNA from McΔ01 (*npa3ΔC*) and MCR03 (*NPA3*) strains for the correct integration of the NATr cassette ( $CTA1_{3'UTR}$ - $TEF1_{5'UTR}$ -*natMX4*- $TEF1_{3'UTR}$ ). Primers #8 and #10 are complementary to the chromosome region flanking the integration site, and primers #9 and #11 pair within the NATr cassette. Finally, mutants were checked for a PCR product of the proper size using primers (#8 / #11) flanking the integration sites. The size of all products obtained in a PCR reaction employing the indicated primers and the genomic DNA isolated from the two recombinant strains **A**) McΔ01 and **B**) MCR03 (*NPA3*), as template, is consistent with the integration having occurred at the expected site by homologous recombination.

Supplemental Figure 2



Comparison between raw and normalized fluorescence values from high fidelity analysis: **A**) comparison for single mutant selection step fluorescence values (KanR); **B**) comparison for double mutant selection step fluorescence values (KanR NatR).

**Supplementary Table 1.** Single and double mutant selection step media for SGA bulk-fluorescence coupled.

	KanR selection	KanRNatR selection
Yeast nitrogen base w/o amino acids and ammonium sulfate (BD Difco)	1.7g	1.7g
Monosodium glutamic acid (Sigma-Aldrich)	1g	1g
Amino acids drop-out mix (-His/Arg/Lys)	2g	2g
Glucose	20g	20g
Agar	20g	20g
Canavanine (100mg/mL) (Sigma-Aldrich)	500uL	500uL
Thialysine (100mg/mL) (Sigma-Aldrich)	500uL	500uL
Hygromycin B (50mg/mL) (Invitrogen)	4mL	4mL
Geneticin (G418) (200mg/mL) (Invitrogen)	1mL	1mL
ClonNAT (100mg/mL) (Werner BioAgents)		1mL
H <sub>2</sub> O to a final volume of	1000mL	1000mL

Ms. No. CUGE-D-21-00136R1

Synthetic negative genome screen of NPA3, a GPN-loop GTPase in *Saccharomyces cerevisiae*

Current Genetics

Dear Dr. Sánchez-Olea,

I am happy to inform you, that your manuscript Synthetic negative genome screen of NPA3, a GPN-loop GTPase in *Saccharomyces cerevisiae* has been accepted for publication in Current Genetics.

The manuscript is now forwarded to Springer for copy and language editing, typesetting and printing. The production department will contact you for proof reading within a couple of weeks.

Thank you for contributing your work to Current Genetics. Please consider us again in the future.

It was accepted on 30 Apr 2022

Thank you for submitting your work to this journal.

With kind regards

Michael-Polymenis


Editor-in-Chief

Current Genetics

## **DIAPOSITIVAS SEMINARIO DE DEFENSA**





  
**UNIVERSIDAD AUTÓNOMA DE SAN LUIS POTOSÍ**  
 FACULTAD DE MEDICINA  
 POSGRADO EN CIENCIAS BIOMÉDICAS BÁSICAS


  
**Función de la GTPasa Npa3 en la levadura *Saccharomyces cerevisiae***

Examen que presenta:  
**M. en C. Martín Antonio Mora García**

Para obtener el grado de:  
**DOCTOR EN CIENCIAS BIOMÉDICAS BÁSICAS**

1



**COMITÉ TUTORAL:**  
**Co-directores de tesis:**  
 Dr. Roberto Sánchez Olea  
 Dra. Mónica Raquel Calera Medina

**Asesoras internas:**  
 Dra. Mariana Salgado Bustamante  
 Dra. Esther Layseca Espinosa

**Asesora externa:**  
 Dra. Lina R. Riego Ruiz

2



**SINODALES:**  
**Presidente sinodal:**  
 Dr. Roberto Carlos Salgado Delgado

**Secretaria sinodal:**  
 Dra. Esther Layseca Espinosa

**Sinodal:**  
 Dra. Mariana Salgado Bustamante

**Sinodal externa:**  
 Dra. Lina Raquel Riego Ruiz

**Sinodal suplente:**  
 Dra. Othir Gidatti Galicia Cruz

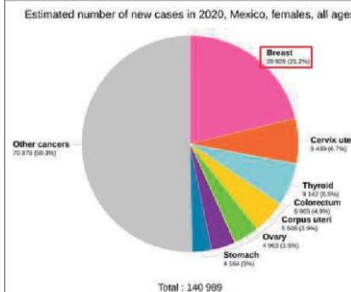
3

**En México el cáncer de mama es el más común entre las mujeres**

En el año 2020 el cáncer de mama fue el tipo de cáncer más diagnosticado en el mundo:
 

- 2,26 millones de nuevos casos.
- 685,000 muertes.

En México, debido al cáncer de mama en el año 2020 fallecieron 7,821 mujeres y 58 hombres.

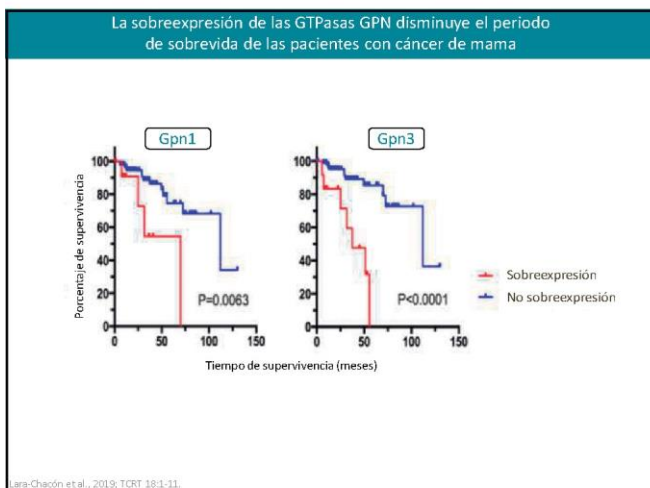


Estimated number of new cases in 2020, Mexico, females, all ages

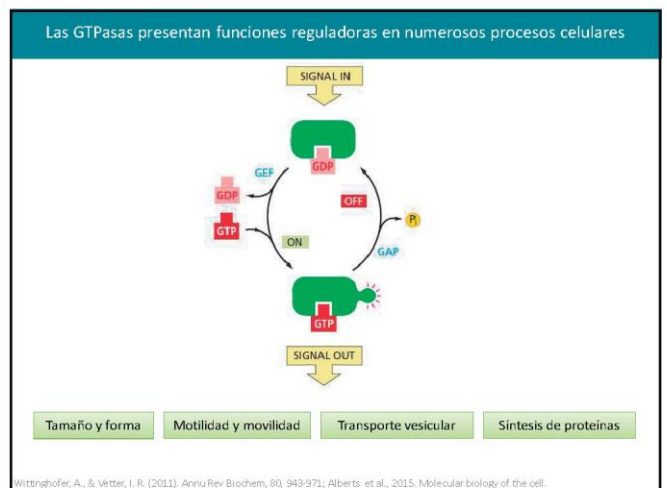
Cancer Type	Number of Cases	Percentage
Breast	2,260,000	21.2%
Other cancers	7,879	0.8%
Cervix uteri	449	0.7%
Thyroid	1,122	2.0%
Colorectum	925	0.8%
Corpus uteri	1,248	0.9%
Ovary	1,923	0.9%
Stomach	1,164	0.9%
<b>Total</b>	<b>1,409,989</b>	

International Agency for Research on Cancer, World Health Organization, INEGI

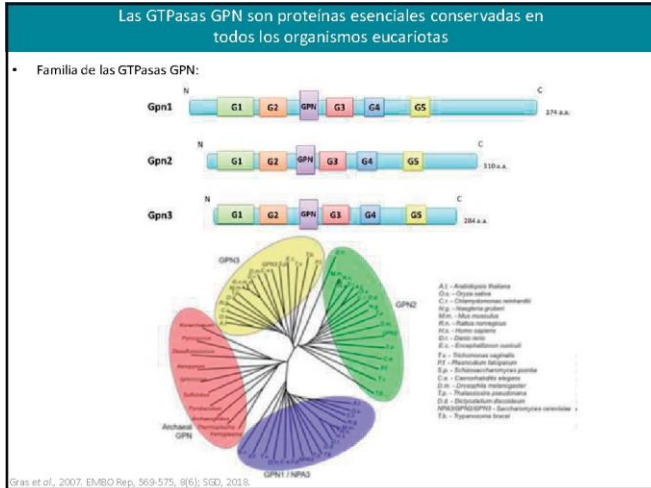
4



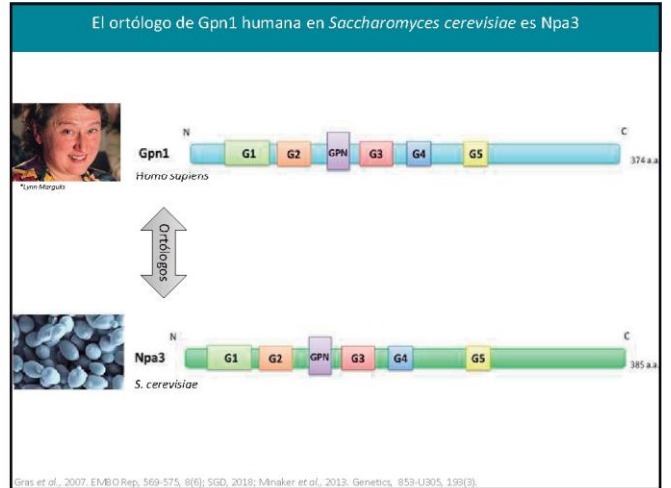
5



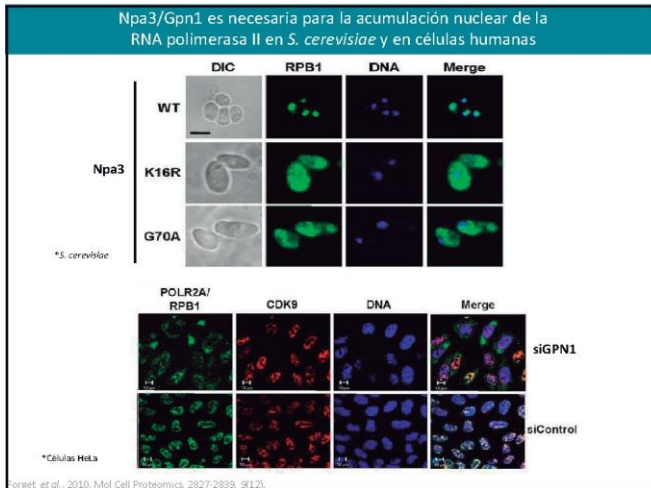
6



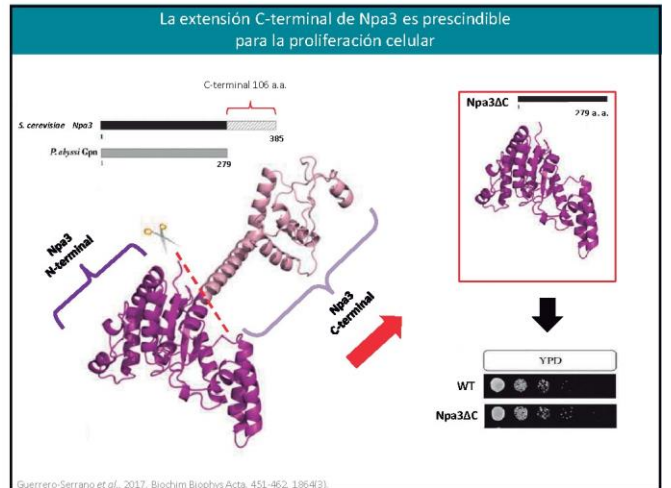
7



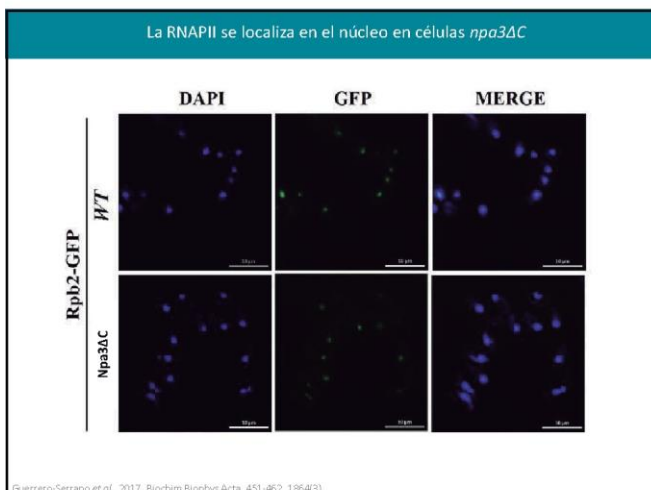
8



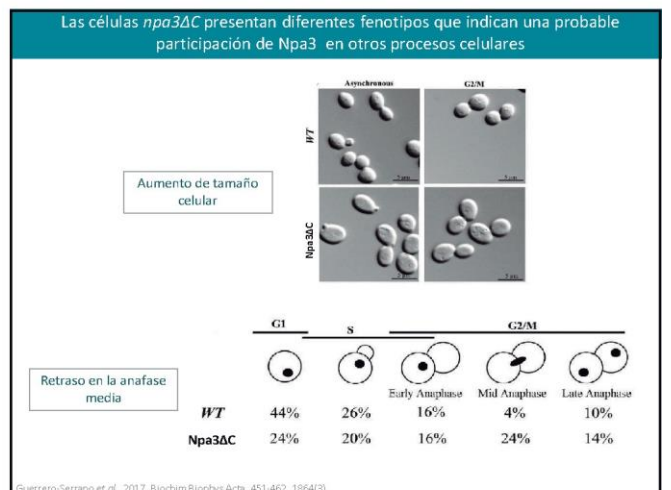
9



10



11



12

La combinación de la mutante *npa3ΔC* con la mutante nula *bik1Δ* produce una interacción genética negativa de letalidad sintética en *S. cerevisiae*

**Bik1 es una proteína de unión a los microtúbulos**

- La delección de BIK1 conduce a una inestabilidad del huso mitótico en anafase.
- Necesario para la elongación de los microtúbulos en la anafase.

Guerrero-Serrano et al., 2017. *Biochim Biophys Acta*, 451-462, 1864-3

13

Las interacciones genéticas se determinan y clasifican al comparar entre los fenotipos de las mutantes simples y mutantes dobles

Existen diferentes mecanismos potenciales que pueden dar origen a interacciones genéticas negativas:

- Miembros redundantes del mismo complejo proteico.
- Miembros del mismo complejo proteico.
- Miembros esenciales de dos complejos que se compensan mutuamente.
- Miembros redundantes de una vía metabólica.
- Miembros con función sinérgica en una vía metabólica.
- Miembros esenciales de vías metabólicas alternativas.

Beyer et al., 2007. *Nature reviews* 9:9-110 (8); Talavera et al., 2013. *PLoS One*, e62866, 8(4).

14

Se generó una cepa recombinante *npa3ΔC* para buscar más interacciones genéticas con *NPA3*

**Disrupción del C-terminal de *NPA3* en el cromosoma.**  
Por recombinación homóloga entre las colas del producto de PCR casete NATr (CTA13 UTR-TEF15 UTR-notMK4-TEF13 UTR) y las regiones homólogas en el cromosoma.

**Selección de clones positivos**  
Exposición a ClonNat (nourseotricina).

Ensayo de dilución por puntos de células en fase estacionaria. OD600 inicial = 0.4 con 5 diluciones seriadas 1:10. Se incubaron a 30°C durante 3 días.

Tesis de maestría Martín Antonio Mora García

15

**Cribado de interacciones genéticas negativas con *npa3ΔC* a nivel de genoma a través de un Arreglo Genético Sintético (SGA)**

Le metodología SGA consiste en cruzar sistemáticamente una cepa de consulta con una colección de mutantes simples para analizar el fenotipo de las mutantes dobles.

Cepa de consulta: *npa3ΔC*

4,389 cepas mutantes por delección en genes no esenciales.

Tesis de maestría Martín Antonio Mora García

16

83 interacciones genéticas negativas con *npa3ΔC* indican una probable participación de *NPA3* en diversos procesos biológicos

Tesis de maestría Martín Antonio Mora García

17

**Hipótesis**

*NPA3* participa en los mismos procesos biológicos de algunos de los genes que presentan una interacción genética negativa con *npa3ΔC*.

18

## Objetivo general

Evaluar la importancia funcional de Npa3 en los procesos biológicos en los que participan los genes que presentan una interacción genética negativa con *NPA3*.

19

## Objetivos específicos

**Objetivo 1**  
 Confirmar las 83 interacciones genéticas negativas con *npa3ΔC* a través de un SGA de alta calidad de réplica.

**Objetivo 2**  
 Analizar la relevancia funcional de las interacciones genéticas negativas de *npa3ΔC*.

20

### La metodología SGA es una herramienta muy útil que permite buscar a gran escala interacciones genéticas en levadura



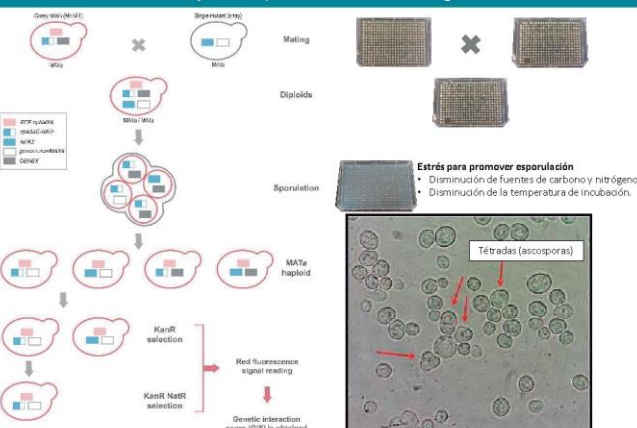

Colección de 4,389 cepas mutantes por delección en genes no esenciales (xxxd)



Laboratorio de sistemas genéticos

21

### El SGA da como resultado mutantes dobles para analizar sus fenotipos de crecimiento en la búsqueda de probables interacciones genéticas



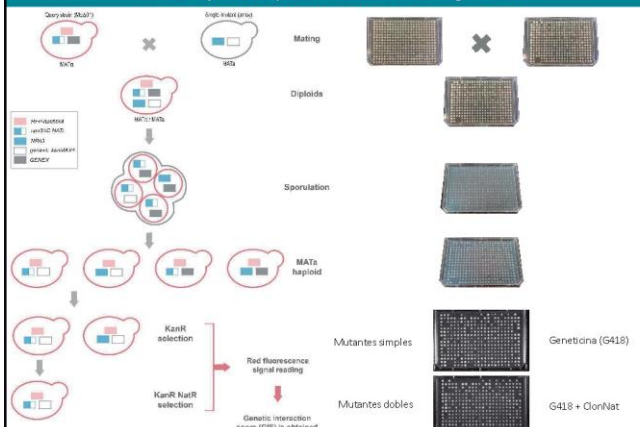
**Estrés para promover esporulación**

- Disminución de fuentes de carbono y nitrógeno.
- Disminución de la temperatura de incubación.

Mora-García et al., 2022. Current Genetics. 68(3-4):343-360.

22

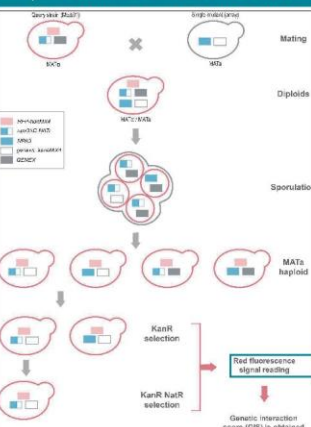
### El SGA da como resultado mutantes dobles para analizar sus fenotipos de crecimiento en la búsqueda de probables interacciones genéticas



Mora-García et al., 2022. Current Genetics. 68(3-4):343-360.

23

### Acoplamiento de la metodología SGA con la detección de la señal de fluorescencia para identificar con alta eficiencia interacciones genéticas negativas de *npa3ΔC*



SGA acoplado a detección de fluorescencia

**YEG01**

• La cepa parental expresa constitutivamente la proteína roja fluorescente mCherry (MATa P<sub>ok1-RFP-*hpMX4*</sub>).

**Parámetros de medición:**

- Excitación: 587 nm
- Emisión: 630 nm
- Flashes [400Hz]: 15

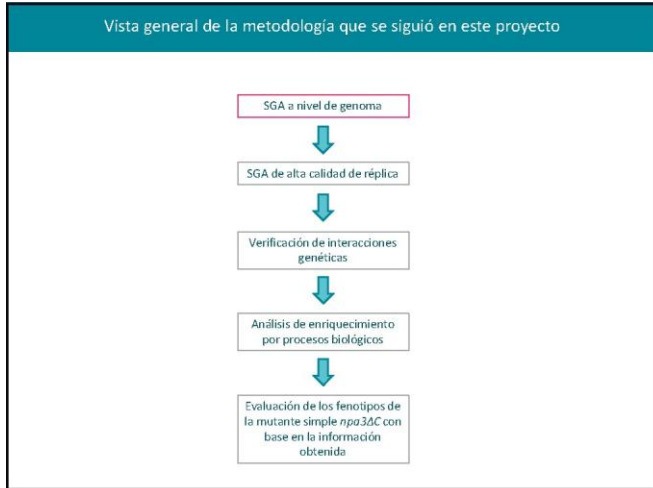
**Lectura de fluorescencia:**

- Parte superior de la placa.
- Matriz de 96 lecturas por posición.
- Tiempo: 430 minutos

TECAN, Infinite M1000

Mora-García et al., 2022. Current Genetics. 68(3-4):343-360.

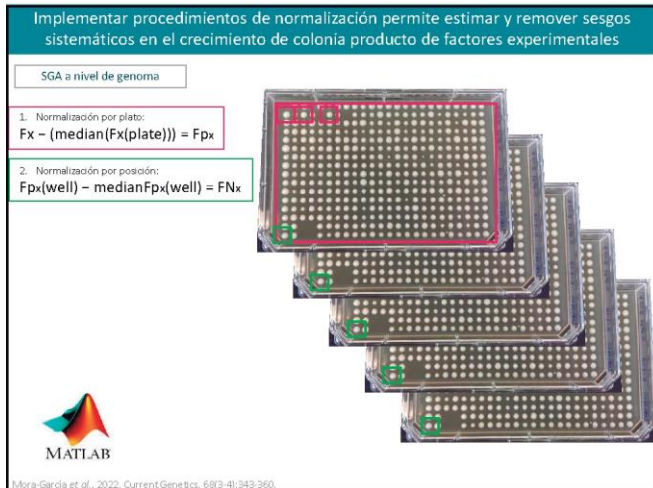
24



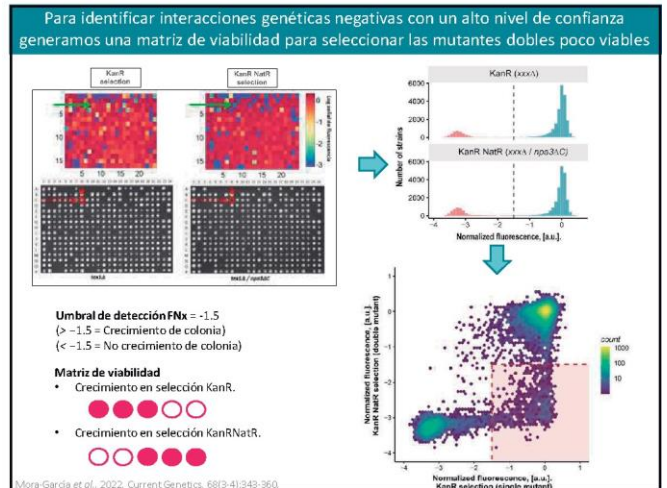
25



26



27



28

Identificamos 83 interacciones genéticas negativas con *npa3ΔC* a través del SGA a nivel de genoma

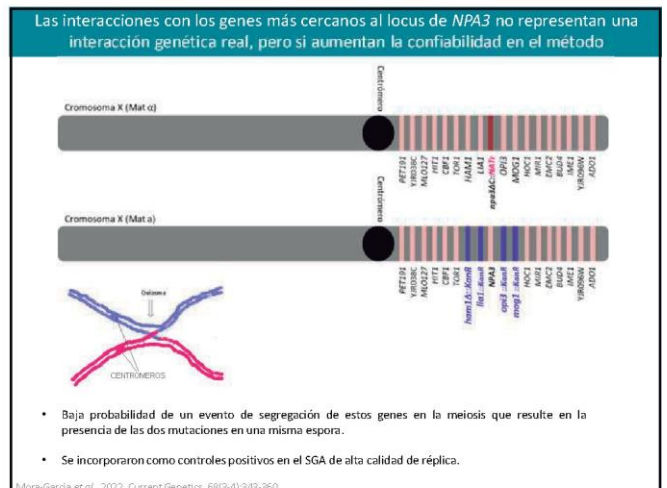
Resultados del SGA a nivel de genoma

**Table 3** Putative negative genetic interactions identified in the *npa3ΔC* genome-wide screening

Putative hits with biological known function		Putative hits with biological unknown function	
ARC18	GAL2	PUF4	WHI5
ATG2	GIS2	RAD33	MTC7
ATG42	GSH1	RAD6	RCI37
ATG8	HAT2	RHO2	RTC4
BDF2	INO2	RIM15	SDD1
BUD27	IZH1	RIM9	SPG3
BUD4	LDS2	RPM4	SRL2
CAF4	LEU9	RRG9	YDR124W
CCC2	MG22	RTS1	YDR094W
CNL1	MIS1	SDD2	YDR491C
COY1	MNN2	SHU2	YDL071C
CUR1	MON2	SIC1	YDR271C
CUS2	MRF1	SMA1	YEL067C
DAL81	MRF137	SPP1	YEL068C
DID4	MSG5	STO1	YFL051C
DLD3	MSW1	SWC5	YGL036W
DNF2	NHP10	TEK1	NRS1
DNL4	PHO80	TPS3	YML012C-A
ELC1	PHO90	UBX2	YNL089C
EFG3	PPA2	VAC8	
FRD1	PPT2	VPS64	

Mora-García et al., 2022, Current Genetics, 68(3-4):343-360

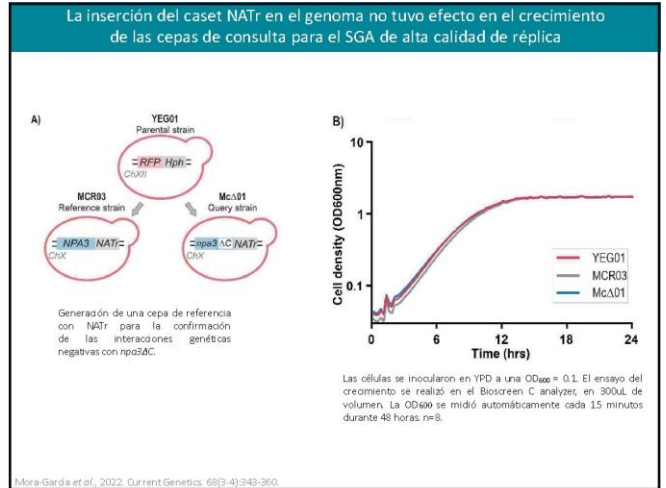
29



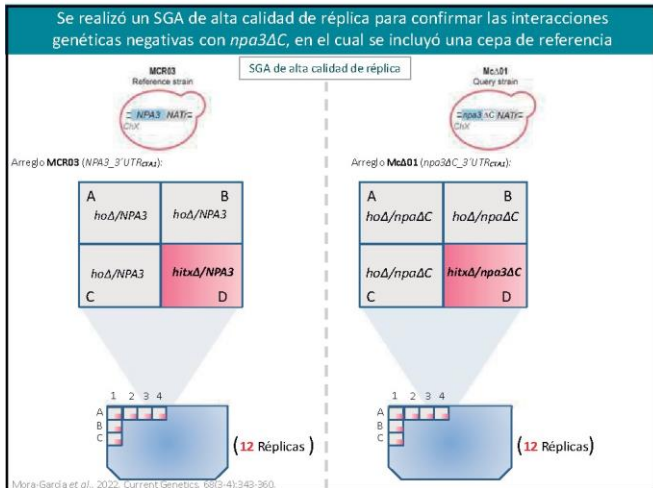
30



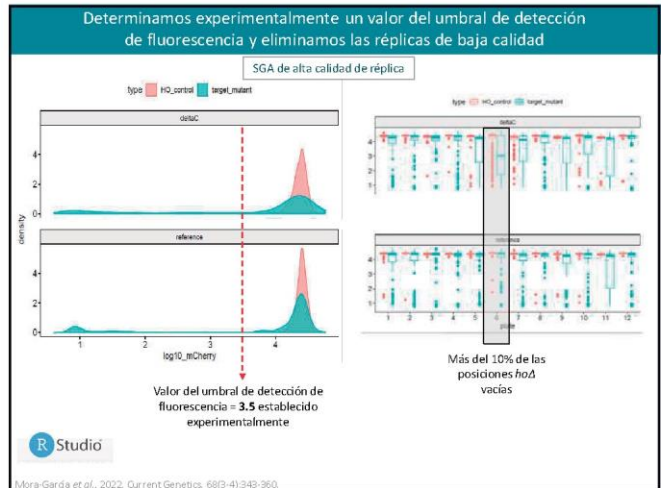
31



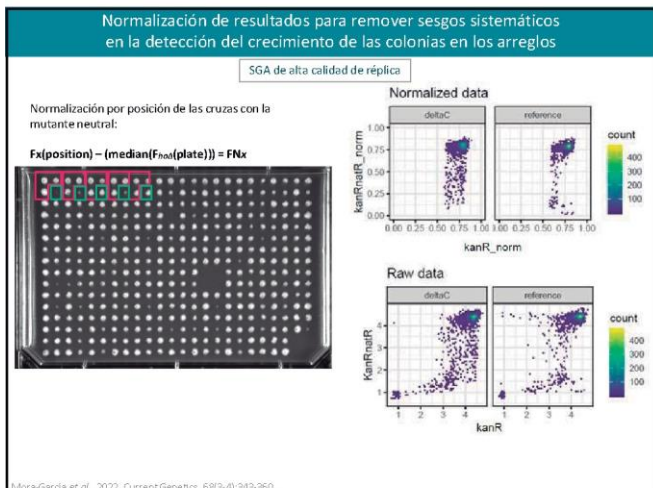
32



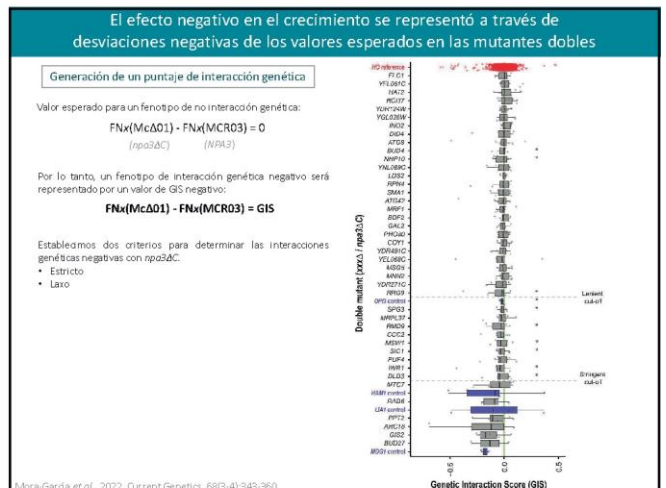
33



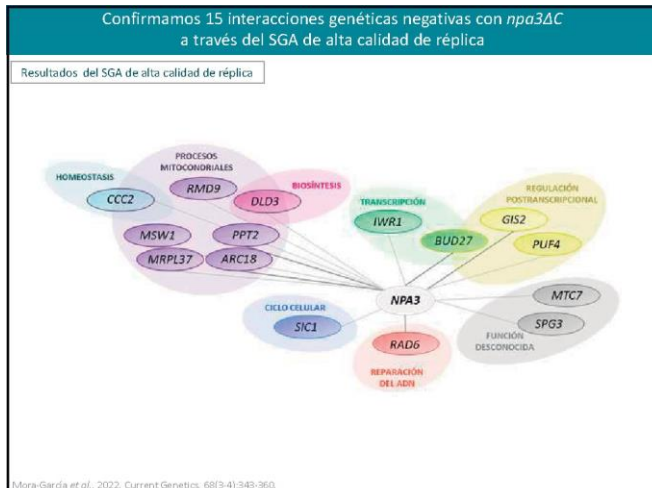
34



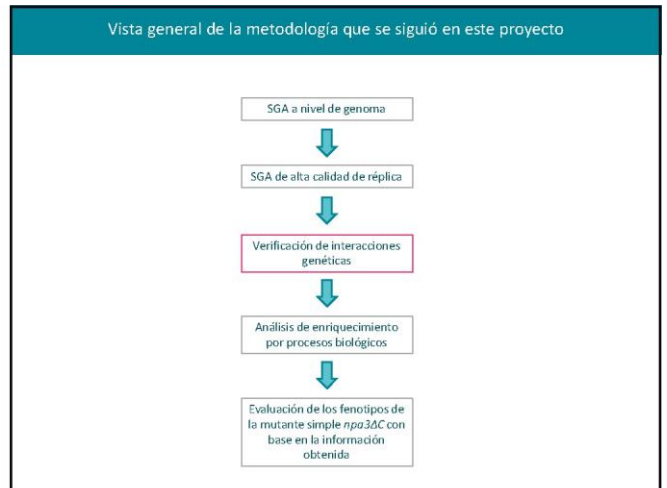
35



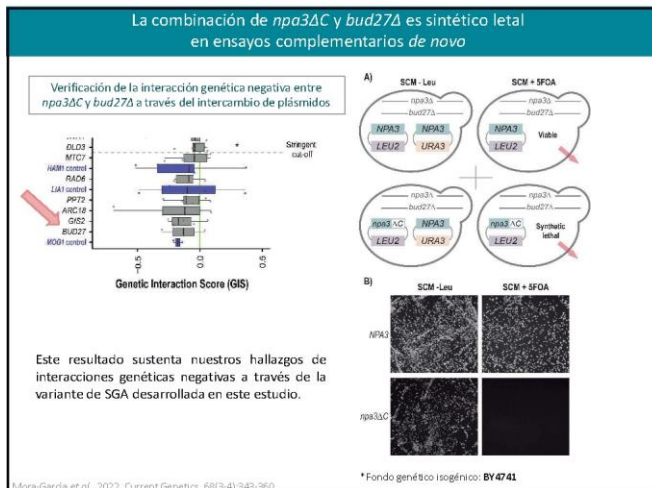
36



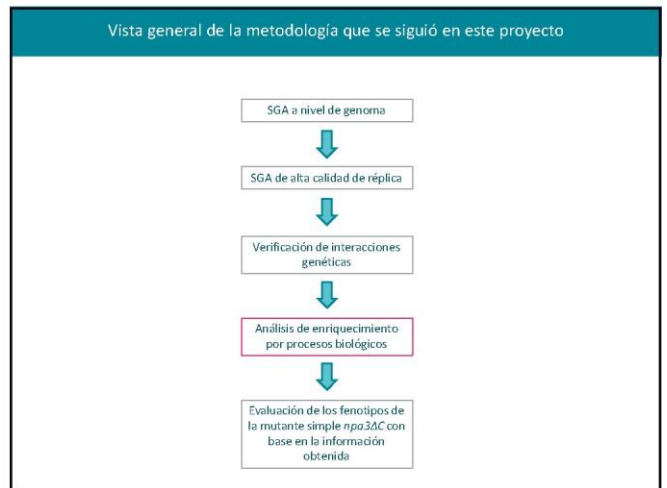
37



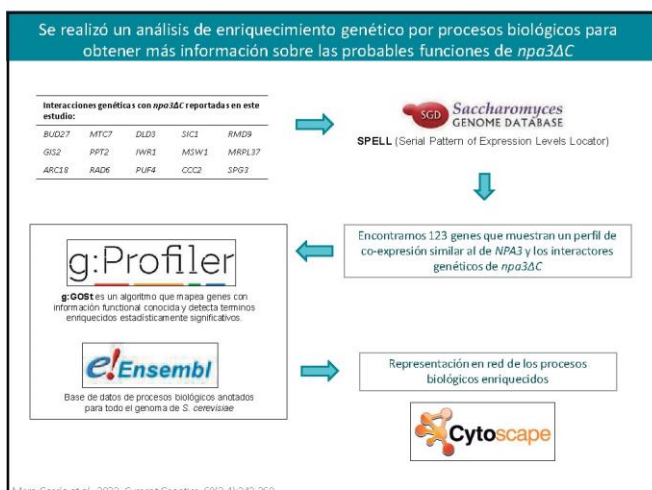
38



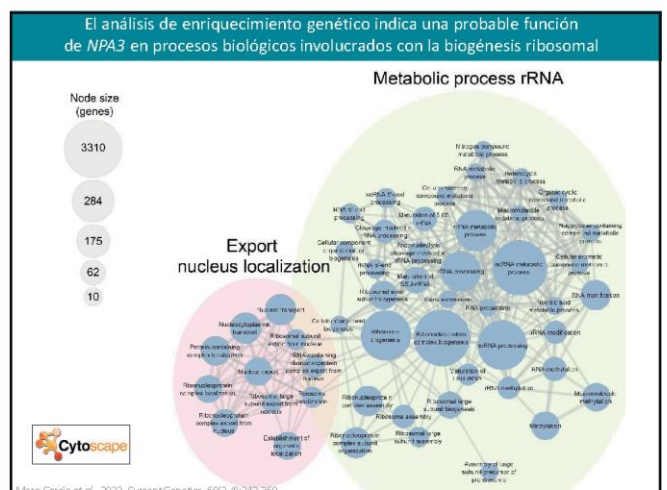
39



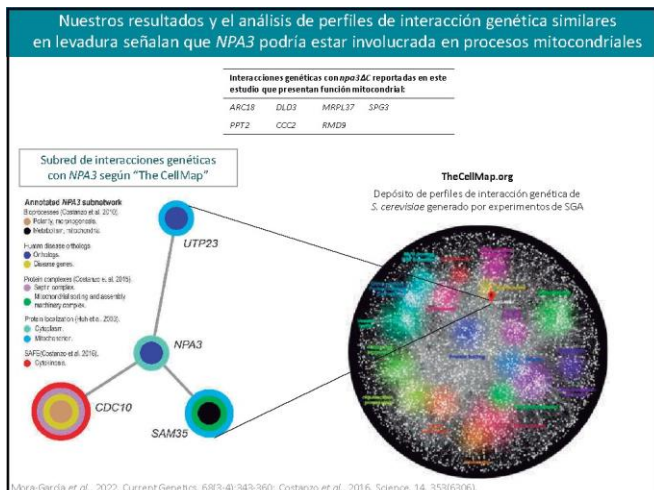
40



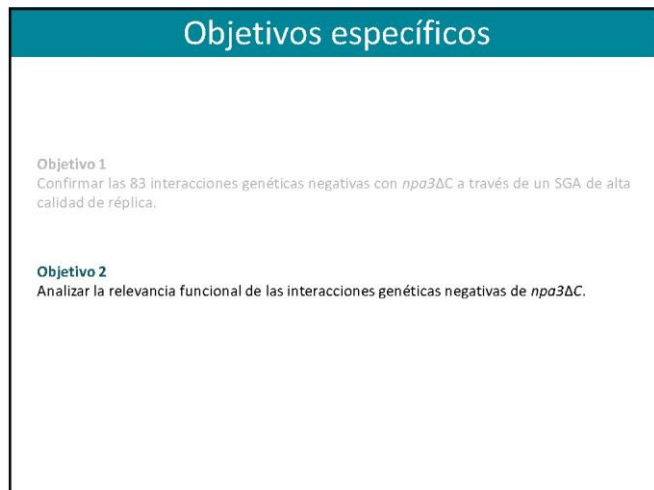
41



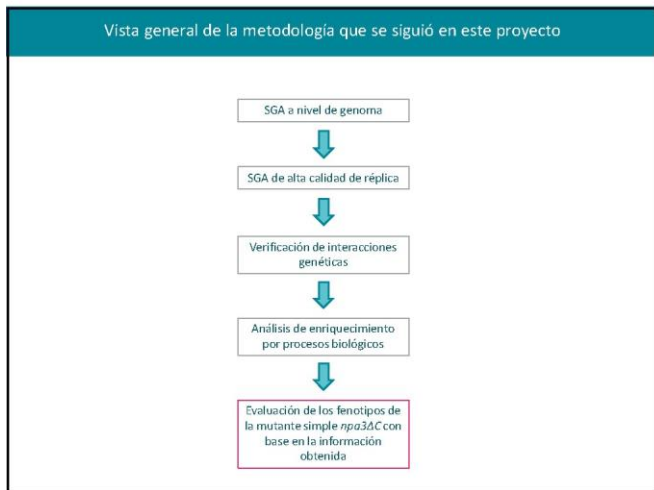
42



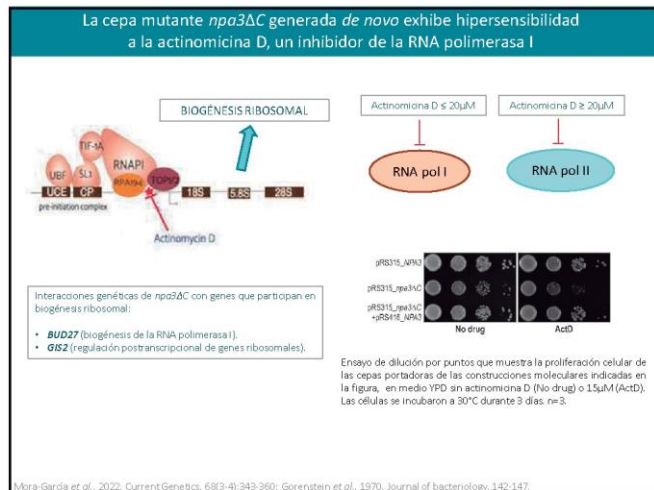
43



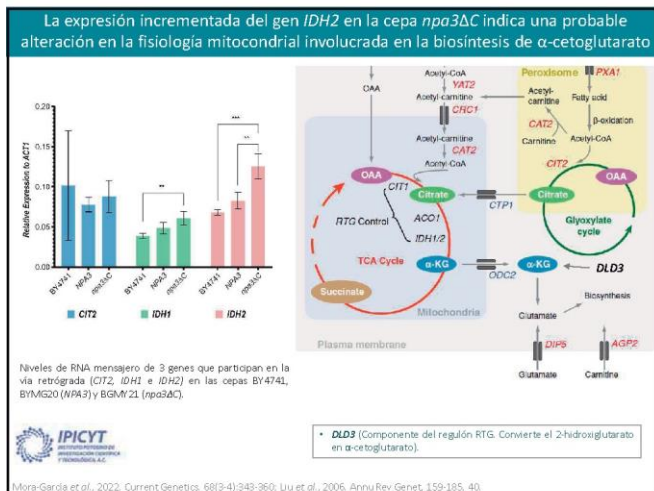
44



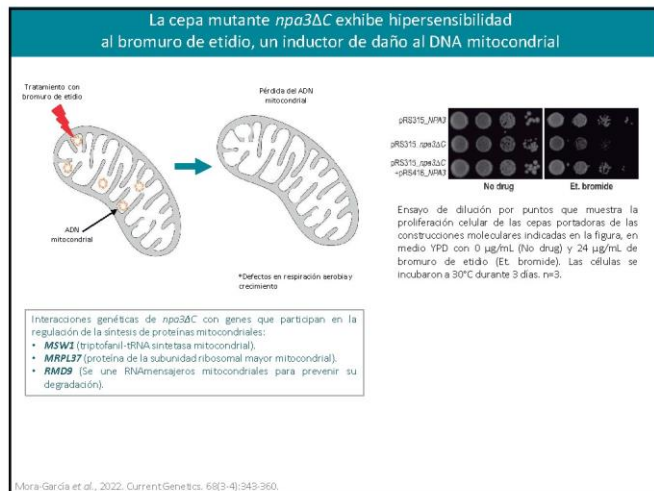
45



46

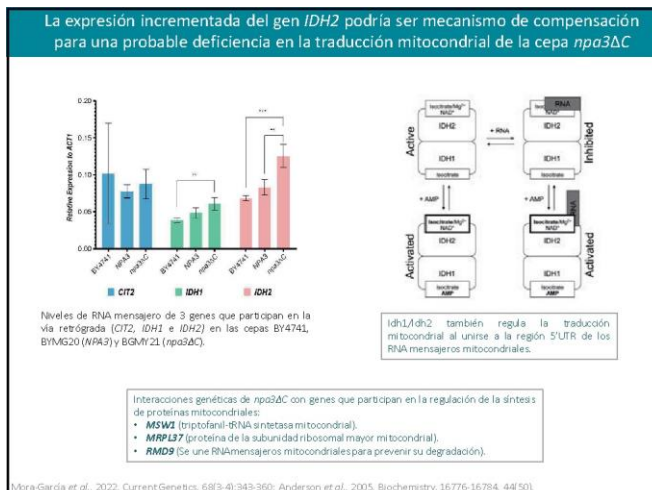


47

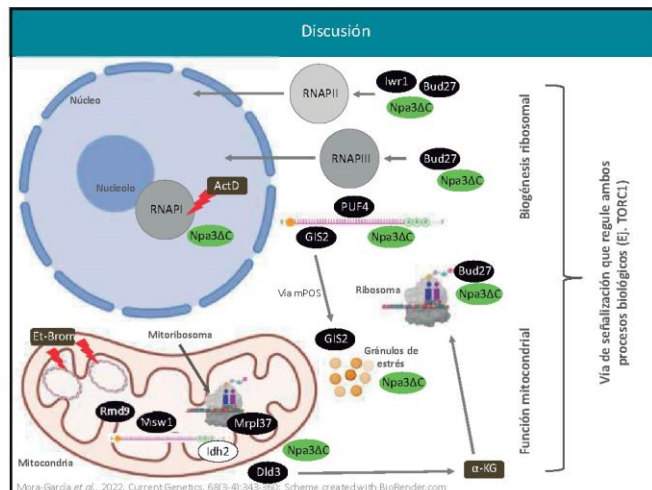


48





49



50

### Discusión

Levadura: *idh1*, *idh2* (Isocitrato deshidrogenasa [IDH])

Humanos: *idh1*, *idh2*, *idh3* (Isocitrato deshidrogenasa [IDH])

- Existe evidencia de que diferentes tipos de mutaciones del gen *IDH2* en humanos están asociadas a diferentes tipos de cáncer de mama:
  - Algunas se asocian con fenotipos agresivos de cáncer de mama.
- Está reportado que la sobreexpresión de *IDH2* en humanos está involucrada en diferentes tipos de cáncer:
  - Endometrio
  - Testicular
  - Próstata
  - Colon

Qiang et al., 2012. *Exp and Ther Med*; Minemura et al., 2021. *Breast Cancer*.

51

### Perspectivas

<i>S. cerevisiae</i>	<i>H. sapiens</i>	Enfermedad asociada
<i>BUD27</i>	<i>URI</i>	Cáncer cervicouterino
<i>GIS2</i>	<i>ZNF9 / CNBP</i>	Distrofia miotónica tipo 2
<i>DLD3</i>	<i>D2HGDH</i>	Aciduria D-2-hidroxiglutarica
<i>CCC2</i>	<i>ATP7A / ATP7B</i>	Asociadas a las enfermedades de Menkes y Wilson respectivamente

\*SGO, 2022.

- Análisis comparativos de la expresión genética entre las cepas que expresan la versión *npa3ΔC* y la versión *NPA3*.
  - Continuar con el enfoque de "alto rendimiento" (microarreglos).
- Análisis comparativos de las interacciones físicas proteína-proteína entre las cepas que expresan la versión *npa3ΔC* y la versión *NPA3*.
  - Continuar con el enfoque de "alto rendimiento" (Ensayos de complementación de fragmentos de proteínas [PCA]).
- Probar experimentalmente si *Npa3* tiene una participación directa en la traducción de proteínas.

52

### Artículos publicados

Current Genetics (2022) 68:343–350  
https://doi.org/10.1007/s00254-022-01243-1

ORIGINAL ARTICLE

#### Synthetic negative genome screen of the GPN-loop GTPase *NPA3* in *Saccharomyces cerevisiae*

Martín Mora-García<sup>1</sup> · Diana Ascencio<sup>2</sup> · Tania Félix-Pérez<sup>2</sup> · Judith Ulloa-Calonzati<sup>2</sup> · Alejandro Juárez-Reyes<sup>2</sup> · Karina Robledo-Marquez<sup>2</sup> · Yolanda Rebolledo-Gómez<sup>2</sup> · Lina Riego Ruiz<sup>2</sup> · Alexander Delana<sup>2</sup> · Mónica R. Calera<sup>2</sup> · Roberto Sánchez-Olea<sup>1</sup>

Received: 27 December 2021 / Revised: 21 April 2022 / Accepted: 30 April 2022 / Published online: 4 June 2022  
© The Author(s), under exclusive license to Springer Nature GmbH Germany, part of Springer Nature 2022

**Abstract**  
The GPN-loop GTPase *Npa3* is encoded by an essential gene in the yeast *Saccharomyces cerevisiae*. *Npa3* plays a critical role in the assembly and nuclear accumulation of RNA polymerase II (RNAPII), a function that may explain its essentiality. Genetic interactions describe the extent to which a mutation in a particular gene affects a specific phenotype when co-occurring with an alteration in a second gene. Discovering synthetic negative genetic interactions has long been used as a tool to delineate the functional relationships between pairs of genes participating in common or compensatory biological pathways. Previously, our group showed that nuclear targeting and transcriptional activity of RNAPII were unaffected in colonies growing exclusively a C-terminal truncated mutant version of *Npa3* (*npa3ΔC*) lacking the last 106 residues normally absent from the single GPN proteins in Archaea, but universally conserved in all *Npa3* orthologs of eukaryotes. To gain insight into novel cellular functions for *Npa3*, we performed here a genome-wide Synthetic Genetic Array (SGA) study coupled to bulk fluorescence monitoring to identify negative genetic interactions of *NPA3* by crossing an *npa3ΔC* strain with a 4,389 nonessential gene-deletion collection. This genetic screen revealed previously unknown synthetic negative interactions between *NPA3* and 15 genes. Our results revealed that the *Npa3* C-terminal tail extension regulates the participation of this essential GTPase in previously unknown biological processes related to mitochondrial homeostasis and ribosome biogenesis.

**Keywords** GTPase *Npa3* · C-terminal deleted *Npa3* · Gpn1 · Synthetic genetic interactions · Synthetic lethal · Fluorescence · Mitochondria · Ribosome biogenesis

53

### Agradecimientos

**GPM team**

- Dr. Roberto Sánchez Olea
- Dra. Mónica R. Calera Medina
- M.C. Tania A. Félix Pérez
- L.Q. Yolanda Rebolledo Gómez
- Diego, Griselda, Karla, Andrea, Julio, Manuel, Alda, Grecia, Ana Karenina, Cristian y Dulce.

**División de biología molecular del IPICYT**

- Dra. Lina R. Riego Ruiz
- Dr. Karina A. Robledo Márquez

**Biología de Sistemas Genéticos (Lab 6) del LANGEBIO**

- Dr. Alexander de Luna Fors
- Dra. Diana I. Ascencio Sánchez
- Dr. Alejandro Juárez Reyes

**Familiares y amigos**

- A mis padres, Rosa y Rafael.

"Fácilmente sigue el hijo las huellas de su padre".

- A mi hijo Rafael Mora.

54